Aging and Disease
www.aginganddisease.org
Early access date: February 18, 2026
http://dx.doi.org/10.14336/AD.2025.1389

Original Article

Receptor-Specific Adenosine Signalling Governs Astrocyte Glycogen Homeostasis

Kaja Belko Parkel[1], Živa Tajda Gržina[1], Robert Zorec[1,2], Marko Kreft[1,2,3*]

[1]Laboratory of Neuroendocrinology-Molecular Cell Physiology, Institute of Pathophysiology, Faculty of Medicine, University of Ljubljana, Ljubljana, Slovenia. [2]Celica Biomedical, Ljubljana, Slovenia. [3]Department of Biology, Biotechnical Faculty, University of Ljubljana, Ljubljana, Slovenia

[Received November 11, 2025; Revised February 4, 2026; Accepted February 5, 2026]

ABSTRACT: Adenosine in the brain rises with metabolic load and signals through A1, A2A, A2B, and A3 receptors, but how individual subtypes regulate astrocytic energy metabolism remains incompletely defined. We combined live-cell FRET sensors for glucose, lactate, and cAMP with Ca^{2+} imaging in primary rat astrocytes to dissect receptor-specific actions. We probed receptor contributions using adenosine and selective agonists (CCPA, A1; CGS21680, A2A; BAY 60-6583, A2B). Glycogen content was quantified by periodic acid–Schiff (PAS) staining after acute stimulation and during recovery from glucose deprivation. Adenosine increased intracellular glucose concentration. Among subtypes, A2B activation reproduced this effect, whereas A1 and A2A did not. However, in glucose-free extracellular solution, adenosine and A2B activation elevated intracellular glucose, implicating glycogenolysis. PAS analysis showed that A2A and A2B increased perinuclear glycogen, with A2B also increasing peripheral glycogen. During recovery from glucose deprivation, adenosine and A2B receptor agonists slowed glycogen replenishment, whereas A2A agonists enhanced perinuclear stores. cAMP concentration rose with A2A and A2B receptor stimulation and after A1 antagonism, but not with adenosine itself, consistent with balanced A1/A2 co-activation. Ca^{2+} responses were transient for adenosine/A1 and sustained for A2A/A2B. Selective A2B activation produced a significant increase in intracellular lactate compared with vehicle. Together, these data identify A2B signalling as a principal driver of acute glucose mobilisation while slowing glycogen replenishment in astrocytes, operating through cAMP elevation and sustained Ca^{2+} signals, whereas A2A preferentially promotes perinuclear glycogen accumulation.

Keywords: A2B adenosine receptor, A2A adenosine receptor, glycogen homeostasis, lactate metabolism, astrocytes

INTRODUCTION

Neurons lack substantial energy reserves and depend on continuous metabolic support. Astrocytes coordinate nutrient uptake, K^+/H^+ homeostasis, and the removal of neuronal metabolites; they also respond to injury and store energy as glycogen [1-4]. Multiple astrocytic G-protein coupled receptors (GPCRs), including adenosine [5-7], cannabinoid [8] and adrenergic [9] receptors, modulate glucose/lactate metabolism and glycogen turnover, but the mechanisms coupling receptor activation to energy substrate handling remain unclear.

While glucose is the recognised brain fuel, astrocytic activation characteristically increases lactate production and release through aerobic glycolysis [10, 11], similar to a Warburg effect in cancer cells [12, 13]. The astrocyte-neuron lactate shuttle (ANLS) hypothesis [14] proposes that astrocyte-derived lactate supports neuronal ATP production [15, 16] and plasticity [17-24]. Glycogen, predominantly astrocytic [25, 26], supplies glucose-6-phosphate for glycolysis and lactate formation and can transiently account for a significant fraction of glucose flux through the "glycogen shunt." In culture, noradrenaline drives lactate production primarily from

***Correspondence should be addressed to:** Dr. Marko Kreft, Institute of Pathophysiology, Faculty of Medicine, University of Ljubljana, Zaloška 4, Ljubljana, Slovenia. Email: marko.kreft@mf.uni-lj.si.

glycogen, whereas basal conditions favour oxidative phosphorylation [9].

Astrocytes also contribute to sleep homeostasis, memory formation, and synaptic plasticity. Sleep is critical for memory consolidation [27] and for re-establishing brain energy balance [28], with broader links between sleep and brain energetics [29]. In this context, adenosine has emerged as a key neuromodulator that couples metabolic load to behaviour: its extracellular levels rise when ATP consumption is high, promoting sleep pressure and fatigue. Early studies identified ATP as an astrocyte-released gliotransmitter [30], and electrophysiological evidence shows Ca^{2+}-dependent vesicular ATP release [31]. In models with impaired astrocytic vesicular release (dnSNARE), extracellular adenosine is reduced, supporting rapid ectonucleotidase-mediated extracellular conversion of astrocyte-derived ATP to adenosine [32-34]. Adenosine may then act through four GPCRs: A1, A2A, A2B, and A3, to shape intracellular cAMP and Ca^{2+} signalling [35].

Work over the past decade has clarified complementary receptor-specific roles. Gliotransmission acting at A1 receptors contributes to the accumulation of sleep pressure [32, 36]. By contrast, A2B signalling in astrocytes has been implicated in tuning energy metabolism to support functions such as sleep and recognition memory: A2B knockdown disrupts hippocampal plasticity, impairs memory, and alters sleep architecture [37].

Mechanistically, adenosine acting via A2B engages the canonical cAMP-PKA pathway to recruit intracellular glucose stores, triggering rapid glycogenolysis followed by delayed glycogen resynthesis in primary astrocytes [38, 39]. The role of A2A receptors on astrocytes remains debated: several groups report astrocytic A2A expression [6, 40, 41], whereas others do not detect Adora2a (A2A gene) in astrocyte RNA-seq datasets [37]. Functionally, A2A signalling can modulate glutamate transport (a metabolically demanding process) and influence memory, but its direct contribution to astrocyte glucose/lactate handling and glycogen metabolism is less clear [41, 42].

Adenosine signalling also intersects with the astrocyte-neuron lactate shuttle (ANLS). Following sleep deprivation, astrocyte gene expression reveals increased transcripts for transporters and enzymes central to ANLS, such as Slc16a1 (encoding MCT1), lactate dehydrogenase A (LdhA), the glucose transporter GLUT1, α2 subunit of Na^+/K^+ ATPase and the glutamate transporter GLT1 [39, 43]. These changes align with the sequence of glutamate uptake and glucose entry proposed in ANLS models [44, 45]. Sleep-wake cycles are accompanied by state-dependent shifts in energy metabolites [46] and by lactate dynamics tracking non-REM slow-wave activity [47-49].

Astrocytes critically coordinate neuronal energy supply by storing glucose as glycogen and by regulating the delivery of energy substrates, such as lactate, to neurons. At the same time, their perivascular and perisynaptic localisation also enables them to contribute to metabolite clearance via the glymphatic pathway [50]. Extracellular adenosine, whose levels fluctuate with neuronal activity and sleep–wake state, can modulate astrocyte morphology and interactions with the cerebrovascular compartment and thus has the potential to influence both metabolic support and glymphatic function [51].

Despite these advances, a comprehensive, receptor-specific view of how astrocytic adenosine signalling coordinates glucose availability, lactate dynamics, glycogen turnover, and second-messenger (cAMP and Ca^{2+}) signalling, particularly under conditions of high ATP consumption and across behavioural states, remains incomplete. Here, we address this gap by combining single-cell FRET nanosensors for glucose, lactate, and cAMP with Ca^{2+} imaging and PAS-based glycogen mapping in cultured rat astrocytes to determine how A1, A2A, and A2B receptor activation shapes astrocyte energy metabolism.

MATERIALS AND METHODS

Cell culture and plasmid transfection

All animal procedures were performed in accordance with the International Guiding Principles for Biomedical Research Involving Animals (Council for International Organisations of Medical Sciences) and the Animal Protection Act (Official Gazette of the RS, No. 38/13, consolidated texts 21/18, 92/20, 159/21). The experimental protocol was approved by the Administration of the Republic of Slovenia for Food Safety, Veterinary and Plant Protection (Republic of Slovenia, Ministry of Agriculture, Forestry and Food, Dunajska cesta 22, 1000 Ljubljana), under permit numbers U34401-27/2020/6, U34401-26/2020/4, and U34401-26/2020/7.

Primary cortical astrocytes were prepared from 2–3-day-old Wistar rats of both sexes, as previously described [52]. For the experiments involving PAS staining of glycogen, primary astrocyte cultures were prepared exclusively from neonatal female rats. For other experiments in this study, primary astrocyte cultures were prepared from mixed-sex litters of neonatal rats. Each experimental series included cells isolated from at least four animals. Mixed cultures were purified by overnight shaking (225 rpm, room temperature) to detach non-astrocytic cells; the procedure was repeated three times until confluent astrocyte monolayers were obtained. Cells

were maintained in high D-glucose DMEM (Dulbecco's Modified Eagle's Medium) supplemented with 10% fetal bovine serum (FBS), 1 mM sodium pyruvate, 2 mM L-glutamine, and 25 µg/mL penicillin-streptomycin in a humidified incubator (95% air / 5% CO_2, 37 °C). Medium was replaced every two days. The purity of astrocyte culture was determined immunocytochemically with antibodies against the astrocytic marker glial fibrillary acidic protein, as previously reported [53].

Purified astrocytes were plated on poly-L-lysine-coated glass coverslips and maintained in culture medium until the experiments. At least 16 hours before the experiments, the cells were transfected with the genetically encoded FRET-based nanosensor (Laconic, FLII12Pglu-700µδ6 or Epac1-camps). The transfection mixture (FuGENE 6 + plasmid DNA) was prepared in antibiotic- and serum-free medium, applied for 2 h at 37 °C, and subsequently replaced with standard culture medium.

Unless otherwise specified, reagents were obtained from Sigma-Aldrich (St. Louis, MO, USA) or Abcam (Cambridge, UK).

Experimental extracellular solutions

The extracellular solutions (ECSs) consisted of 135.3 mM NaCl, 5 mM KCl, 10 mM HEPES (4-(2-hydroxyethyl)-1-piperazineethanesulfonic acid), 0.5 mM $NaH_2PO_4 \times H_2O$, 5 mM $NaHCO_3$, 2 mM $MgCl_2$, 1.8 mM $CaCl_2$ and 3 mM D-glucose; the pH was adjusted to 7.2 with NaOH. The osmolarity of the solution, measured with a freezing-point osmometer (Osmomat 030; Gonotec GmbH, Berlin, Germany), was 290-310 mOsm. Changes in osmolarity were compensated with NaCl. For positive-control experiments, the ECS composition was modified to include either additional glucose or lactate. Specifically, 95.3 mM NaCl, 5 mM KCl, 10 mM HEPES, 0.5 mM $NaH_2PO_4 \times H_2O$, 5 mM $NaHCO_3$, 2 mM $MgCl_2$, 1.8 mM $CaCl_2$, 3 mM D-glucose were combined with the appropriate amount of 40 mM D-glucose or 40 mM L-lactate stock solution to maintain the osmolarity within the same range (290–310 mOsm, pH 7.2). For cAMP measurements, 100 µM noradrenaline (NA) diluted in ECS served as a positive control.

For monitoring changes in intracellular metabolites and secondary messengers following stimulation of adenosine A1, A2A, A2B receptors, 100 nM 2-Chloro-N^6-cyclopentyladenosine (CCPA), 100 nM 3-(4-(2-((6-amino-9-((2R,3R,4S,5S)-5-(ethylcarbamoyl)-3,4-dihydroxy tetrahydrofuran-2-yl)-9H-purin-2-yl)amino) ethyl)phenyl)propanoic acid (CGS21680) or 1 µM [2-((6-amino-3,5-dicyano-4[4-(cyclopropylmethoxy) phenyl] pyridine-2-yl)sulfanyl)acetamide] (BAY 60-6583) agonist solution was used, each diluted in ECS. To monitor changes after the stimulation of all adenosine receptors, 100 nM adenosine solution was applied. In cAMP experiments, 800 nM 8-cyclopentyl-1,3-dipropylxanthine (DPCPX) antagonist solution was added, following preincubation in 100 nM adenosine solution. For A2B receptor antagonism, astrocytes were preincubated for 30 minutes at 37 °C in ECS containing 10 µM PSB-603 (8-(4-[4-(4-chlorophenyl)piperazine-1-sulfonyl]phenyl)-1-propyl-2,3,6,7-tetrahydro-1H-purine-2,6-dione). Where indicated, PSB-603 was present throughout recording and included in all agonist solutions (where applicable). For equilibrative nucleoside transporter (ENT) inhibition, astrocytes were preincubated for 30 min at 37 °C in ECS containing 10 µM dipyridamole and was present throughout recording.

We used ligand-specific concentrations to approximate EC_{80} for each receptor in astrocytes, guided by IUPHAR values and prior cell-based assays. For A_1, CCPA 100 nM (K_i ~1–2 nM at rat/human A_1) ensures >95% occupancy. For A2A, CGS21680 100 nM corresponds to ~80% occupancy given K_i ~20–30 nM. For A2B, we used BAY 60-6583 1 µM because A2B is a low-affinity receptor for adenosine and BAY 60-6583 is a partial agonist with variable apparent potency across species (K_i = 10-330 nM); 1 µM reliably elicits A2B responses in primary cells, ensuring 75-99% occupancy [54-58]. For A2B antagonism, we used PSB-603 10 µM, a highly selective A2B antagonist (K_i = 0.553 nM) [37], providing effectively saturating blockade under our conditions. For ENT inhibition, we used dipyridamole 10 µM (reported ENT1 K_i = 8.18 nM) [59], a concentration well above reported inhibitory constants and therefore expected to yield near-complete suppression of ENT-mediated adenosine uptake.

Immunocytochemistry

To confirm the presence of adenosine receptors in primary astrocyte cultures, immunocytochemistry was performed. Astrocytes were seeded onto poly-L-lysine-coated glass coverslips 1-3 days before the experiment. The cells were rinsed with PBS and fixed in formaldehyde prepared from 4% paraformaldehyde in PBS for 25 minutes. After washing four times with PBS, nonspecific staining was blocked by incubation in 3% bovine serum albumin (BSA) and 10% goat serum in PBS for one hour at 37 °C. Because the immunostaining protocol omits detergent permeabilization, the antibodies are expected to primarily label receptor epitopes accessible from the extracellular side of the plasma membrane; therefore, Figure 1 should be interpreted as reporting surface-accessible receptor expression under these conditions. Cells were then washed with PBS and then incubated overnight at 4°C with rabbit anti-A1 (Abcam; ab82477), anti-A2A

(Abcam; 260032) or anti-A2B (Sigma Aldrich; AB1589P) adenosine receptor primary antibodies, diluted 1:400, 1:100, 1:200 (respectively) in PBS containing 3% BSA. No antigen retrieval was performed for any of the adenosine receptor immunostainings. The following day, the cells were washed with PBS and incubated with Alexa Fluor 488-labelled goat anti-rabbit secondary antibodies, diluted in PBS containing 3% BSA for 45 minutes at 37 °C at a dilution of 1:600. After washing four times with PBS, coverslips were mounted in Slowfade Gold antifade (Invitrogen, Cat. No. S36942) and observed by the confocal microscope (Zeiss LSM700 AxioObserver; Plan Apochromat 63×/1.4 NA oil immersion lens) with excitation via diode laser at 488 nm and emission signal filtered with long pass filter at 496-800 nm. Control experiments using secondary antibodies alone produced no detectable fluorescent signal, confirming the specificity of the immunolabeling.

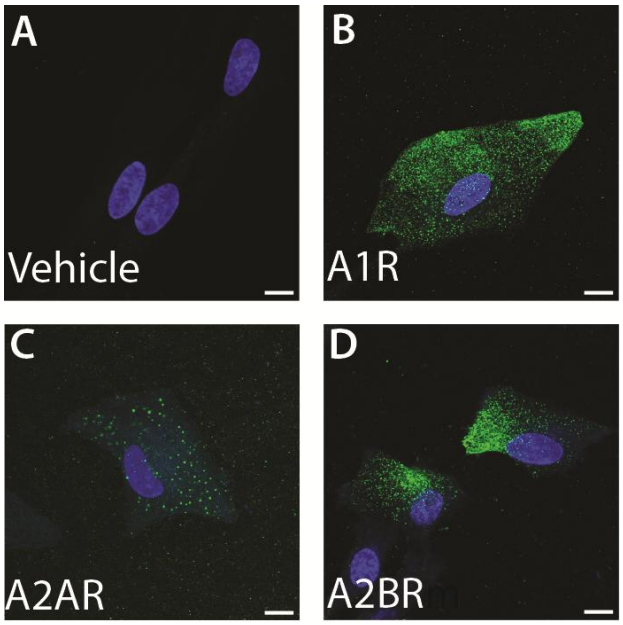

Figure 1. Immunoreactivity for adenosine A1, A2A and A2B receptors is detected in cultured astrocytes. Immunocytochemical detection of adenosine receptors (green) in primary rat astrocytes, fluorescently labelled with antibodies against A1 **(B)**, A2A **(C)** and A2B **(D)**. Secondary-only control: no specific fluorescence detected **(A)**. Scale bar: 10 µm, blue: DAPI.

FRET imaging and analysis

The Förster resonance energy transfer (FRET) technique was used to monitor, in real time, intracellular glucose, lactate, and cAMP levels in single astrocytes. Transfected astrocytes were incubated for 30 minutes in standard extracellular solution (ECS) and then mounted in a custom recording chamber containing 200 µL ECS. After a 5-minute baseline recording, an equal volume (200 µL) of either vehicle or agonist solution was added. All agonists were prepared at 2× concentration in ECS so that, after addition of an equal volume to the chamber, the final bath concentration matched the stated value. Recordings continued for an additional 10 min, followed by application of 400 µL of the appropriate control solution to verify sensor responsiveness. Imaging was conducted 16-30 hours post-transfection on a fluorescence microscope (Zeiss Axio Observer.A1; Zeiss, Oberkochen, Germany) with C-Apochromat 63×/1.2 NA water objective (Zeiss) and a camera (Axiocam 702 mono, Zeiss). Image acquisition was performed with Zeiss Zen software. Cells were excited by an LED light source (Colibri.2, Zeiss) at 445 nm. Emitted fluorescence was separated into cyan (460 nm) and yellow (520 nm) channels by an image splitter (Photometrics DV2; Optical Insights, Tucson, AZ, USA). Images were acquired every 5 seconds for cAMP measurements and every 10 seconds for glucose and lactate measurements, with 100-200 ms exposure times. For the glucose sensor (FLII12Pglu-700µδ6), changes in intracellular glucose concentration were calculated as variations in the YFP/CFP ratio, where an increase in ratio corresponds to a rise in $[glucose]_i$. For cAMP (Epac1-camps) and lactate (Laconic) sensors, the CFP/YFP and mTFP/Venus ratios were used, respectively. Because these sensors respond inversely (a decrease in YFP/CFP or Venus/mTFP reflects an increase in analyte concentration), data were reported as CFP/YFP and mTFP/Venus ratios, ensuring that an increase in ratio consistently represents an increase in $[cAMP]_i$ or $[lactate]_i$, respectively. For each cell, a baseline FRET ratio was defined as the mean value over a 100 s pre-stimulus period. Changes are reported as percent change relative to baseline.

Periodic acid-Schiff staining

Cytosolic localisation of glycogen was assessed with the modified Periodic Acid-Schiff (PAS) method [60] using the Periodic Acid-Schiff kit, with modifications for cell cultures as previously described [9]. Cells were plated on poly-L-lysine-coated coverslips 2 days before the experiment. After treatments at 37 °C (30 min pre-incubation in ECS or agonist solution; 120 min glucose deprivation, 120 min glucose deprivation + 120 min recovery in ECS, 120 min glucose deprivation + 120 min recovery in agonist solution), cells were washed with ice-cold PBS and fixed with formaldehyde prepared from 4% paraformaldehyde in PBS for 15 minutes and formaldehyde with 0.1% Triton X-100 for 10 min at room temperature and washed four times with PBS. After a 5-minute incubation at room temperature in 1% (w/v) periodic acid solution, the cells were washed under

running deionised water and stained with Schiff's reagent for 30 minutes at room temperature. After staining, the cells were rinsed under running deionised water, dehydrated in an alcohol series from 70% to 100% ethanol and mounted with Eukitt® Quick hardening mounting medium.

Fluorescent images were acquired with a fluorescent microscope (Zeiss Axio Observer.A1; Zeiss) equipped with C-Apochromat 63×/1.2 NA water immersion objective (Zeiss) and a CMOS camera (Axiocam 702 mono, Zeiss). Cells were illuminated using a Colibri 7 LED light source (Zeiss) at 555 nm excitation, and fluorescence emission was collected through a BP 605/70 filter. Exposure time was 1000 ms for all recordings. Images were obtained across the entire coverslip to ensure representative sampling. Regions of interest (ROIs) were manually delineated around each cell (excluding the nucleus), and fluorescence intensity was quantified using ZEN (Zeiss) and ImageJ (NIH) software. The mean fluorescence intensity per cell was calculated as the average of all pixel intensities within each ROI.

Calcium measurements

Intracellular calcium dynamics were monitored using the high-sensitivity fluorescent Ca^{2+} indicator CAL520-AM, dissolved in DMSO to 5 mM and stored at -20 °C until use. Before the experiments, the stock solution was diluted in culture medium to a final concentration of 5 µM. Cells were plated on poly-L-lysine-coated coverslips 2 days before the experiment. On the day of the experiment, the coverslips were incubated for 20-30 minutes in 5 µM CAL520-AM solution at 37 °C to allow the dye to enter the cells. After the loading period, the medium was replaced with extracellular solution and left in the dark at room temperature for an additional 30 minutes. During this period, intracellular esterases cleaved the acetoxymethyl (AM) groups, trapping the fluorescent, negatively charged CAL520 within the cytosol. The dye's fluorescence intensity increases upon binding Ca^{2+}, allowing real-time quantification of intracellular calcium changes.

Coverslips with astrocytes were mounted onto the microscope's recording chamber. Recordings were acquired with a fluorescent microscope (Zeiss Axio Observer.A1; Zeiss, Oberkochen, Germany) with C-Apochromat 63×/1.2 NA water objective (Zeiss) and a camera (Axiocam 702 mono, Zeiss). Cells were excited by a LED light source (Colibri.2, Zeiss) at 490 nm. Emitted fluorescence was filtered at 509 nm and imaging was performed with Zeiss Zen software. Images were acquired every 3 seconds with an exposure time of 150 ms. The mean fluorescence intensity within each ROI was measured, excluding the nucleus.

Statistical analysis

Unless otherwise stated, all results are presented as mean ± standard error of the mean (SEM). Statistical analyses were performed using SigmaPlot 11.0 (Systat Software, USA), Microsoft Excel, and custom Python scripts. For comparisons between two groups, statistical significance was assessed using a two-tailed Student's t-test when data met assumptions of normality and equal variance (verified by Shapiro–Wilk and Levene's tests). When these assumptions were violated, the Mann-Whitney U test was applied. For comparisons involving more than two groups, a one-way analysis of variance (ANOVA) was used, followed by appropriate post hoc tests where indicated. Differences were considered statistically significant at $p < 0.05$, $p < 0.01$, and $p < 0.001$, and are denoted in figures by one, two, or three asterisks, respectively. In box-and-whisker plots, the box represents the interquartile range (IQR, middle 50% of the data); the horizontal black line marks the median, the red line indicates the mean, and whiskers extend to the 10^{th} and 90^{th} percentiles. Sample sizes (n) are shown in figure legends or adjacent to each box.

RESULTS

Immunocytochemical Detection of Adenosine Receptors on Astrocytic Membranes

To determine whether cultured rat astrocytes express adenosine receptors, we performed immune-cytochemistry for A1, A2A, and A2B subtypes. Confocal imaging revealed immunoreactivity for all three receptors (Fig. 1), consistent with previous reports [61, 62], but see [37] for RNA-seq data suggesting relatively low A2A expression. Qualitatively, the A2A signal appeared lower than the A1 and A2B under identical imaging conditions. Negative controls processed identically but without primary antibodies showed no detectable fluorescence, supporting the specificity of the labelling. Taken together with prior work, these data indicate that our cultured astrocytes express A1, A2A and A2B receptors at levels sufficient to support the pharmacological experiments described below, while not addressing the broader quantitative debate on astrocytic A2A expression.

Adenosine receptor stimulation increases $[glucose]_i$ in cultured astrocytes

We next quantified how adenosine receptor activation affects intracellular glucose in single astrocytes using the genetically encoded glucose FLII12Pglu-700µδ6 FRET nanosensor. Each recording comprised a 300 s baseline, followed by bath addition of vehicle or agonist and

continued imaging for 600 s; 10 mM D-glucose was applied at the end of each experiment to verify sensor responsivity. For summary statistics, amplitudes were computed over the final 100 s of the recording.

Astrocytes were stimulated with adenosine (100 nM; non-selective adenosine receptor agonist; Fig. 2A-C), CCPA (100 nM; A1 agonist; Fig. 2D-F), CGS21680 (100 nM; A2A agonist; Fig. 2G-I), or BAY 60-6583 (1 µM; A2B agonist; Fig. 2J-L). For vehicle controls, an equal volume of ECS was added to the bath to match handling and mechanical perturbation.

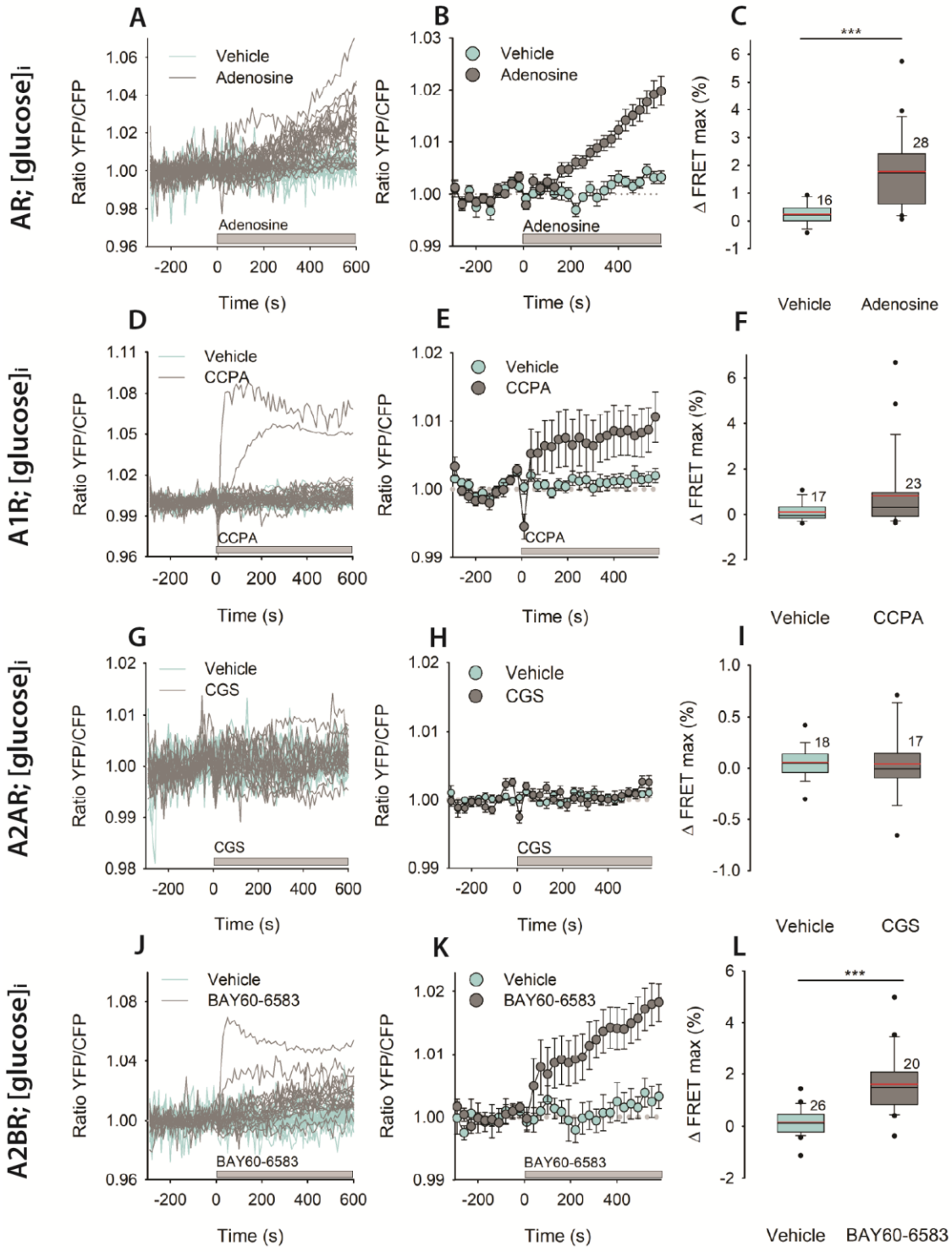

Figure 2. Adenosine receptor activation increases intracellular glucose in cultured rat astrocytes. Astrocytes were stimulated with adenosine (100 nM, non-selective; **A-C**), CCPA (100 nM, A1; D-F), CGS21680 (100 nM, A2A; **G-I**), or BAY 60-6583 (1 µM, A2B; J-L); vehicle = ECS. Time 0 indicates the addition of the vehicle/agonist. The left panels (**A, D, G, J**) represent single-cell FLII12Pglu-700µδ6 YFP/CFP ratio traces normalised to baseline (vehicle, blue; agonist, grey). The middle panels (**B, E, H, K**) represent mean ± SEM traces corresponding to the left panels. The right panels (C, F, I, L) represent summary amplitudes (mean ± SEM) computed over the final 100 s of the recording. Increases in YFP/CFP reflect higher $[glucose]_i$. Mann-Whitney U test versus matched vehicle for each condition. Adenosine increased $[glucose]_i$ (Δ 1.77 ± 0.25% vs 0.24 ± 0.10%; U = 51, $p < 0.001$). CCPA and CGS21680 showed no significant effect (U = 132 and U = 140, respectively). BAY 60-6583 increased $[glucose]_i$ (Δ 1.60 ± 0.27% vs 0.17 ± 0.10%; U = 46, $p < 0.001$). n denotes independently analysed single cells.

Bath application of adenosine (100 nM) significantly increased the YFP/CFP FRET ratio relative to vehicle, corresponding to a rise in intracellular glucose, $[glucose]_i$ (Δ 1.77 ± 0.25% vs 0.24 ± 0.10%; Mann-Whitney U = 51, $p < 0.001$; n = 28 vs 16). Individual-cell traces showed a consistent upward deflection after adenosine, whereas vehicle responses remained near baseline.

Selective activation of A1 with CCPA (100 nM) produced no significant change in $[glucose]_i$ compared with vehicle (0.82 ± 0.35% vs 0.10 ± 0.10%; U = 132, n.s.; n = 17 vs 23). Notably, a higher CCPA concentration (1 µM) elicited a small but significant increase (0.6 ± 0.1%; n = 29), though subtype selectivity is likely reduced at this dose.

Selective activation of A2A receptor with CGS21680 (100 nM) also failed to significantly alter $[glucose]_i$ compared with matched vehicle controls (0.04 ± 0.08% vs 0.05 ± 0.04%; U = 140, n.s.; n = 17 vs 18). Traces largely overlapped with vehicle, suggesting minimal acute impact of A2A activation on cytosolic glucose under these conditions.

In contrast, the selective A2B agonist, BAY 60-6583 (1 µM), produced a robust increase in $[glucose]_i$ (Δ 1.60 ± 0.27% vs 0.17 ± 0.10%; U = 46, $p < 0.001$; n = 20 vs 20). Single-cell traces showed a rapid rise after agonist addition, which persisted throughout the analysis window.

The pattern across subtypes indicates that the adenosine-evoked increase in $[glucose]_i$ is predominantly mediated by A2B receptors under our experimental conditions. The lack of effect with 100 nM CCPA and CGS21680 argues against significant contributions from A1 or A2A at these doses and time scales. Even if A2B occupancy at 100 nM adenosine is only partial, the close match between adenosine- and BAY 60-6583-evoked $[glucose]_i$ responses, together with the glycogen, cAMP and Ca^{2+} data, supports A2B as the primary contributor to adenosine's acute metabolic effect under our conditions.

Subsequent experiments under glucose-free ECS and further support a glycogenolytic origin for the A2B-dependent signal.

Stimulation of adenosine A2 receptors leads to increased glycogen accumulation

To quantify glycogen, we measured PAS fluorescence intensity in single astrocytes (arbitrary units, a.u.). Because staining was spatially heterogeneous, higher perinuclearly than at the periphery, we analysed three predefined square ROIs per cell: ROI_1, adjacent to (but excluding) the nucleus, and ROI_2 - ROI_3 positioned along the short cell axis toward the periphery, as shown in Supplementary Fig. 1. Figure 3A reports perinuclear intensity (ROI_1); Figure 3B reports the most peripheral intensity (ROI_3); Figure 3C shows the perinuclear/periphery ratio (ROI_1/ROI_3), indexing perinuclear enrichment.

Astrocytes were pre-treated for 30 min at 37 °C with vehicle (ECS) or one of four agonists: adenosine (100 nM; all ARs), CCPA (100 nM; A1R), CGS21680 (100 nM; A2AR), or BAY 60-6583 (1 µM; A2BR). Cells were then fixed and processed for PAS staining (Methods 2.5).

A2A (n = 156) and A2B (n = 149) stimulation significantly increased PAS intensity versus vehicle, whereas A1 agonist (n = 121) and adenosine did not differ from vehicle (Fig. 3A), Kruskal–Wallis H = 50.803, df = 4, $p < 0.001$; Dunn's post hoc: A2A > vehicle, A2B > vehicle (both $p < 0.001$); adenosine, vehicle (n.s.). Only A2B increased peripheral PAS intensity (Fig. 3B); A1, A2A, and adenosine were not different from vehicle, H = 11.243, df = 4, p = 0.024; Dunn's: A2B > vehicle ($p < 0.05$). The ROI_1/ROI_3 ratio (Fig. 3C) increased after A2A (perinuclear-biased accumulation), while A2B raised both compartments and therefore did not increase the ratio to the same extent, H = 22.022, df = 4, $p < 0.001$; Dunn's: A2A > vehicle ($p < 0.001$). Together, these data indicate that A2 receptor activation promotes glycogen accumulation, with A2A favouring perinuclear enrichment and A2B increasing glycogen both perinuclearly and at the periphery.

A2B receptor-driven glycogenolysis increases $[glucose]_i$ under glucose-free conditions

To discriminate glucose influx from glycogenolysis, we repeated the FLII12Pglu-700µδ6 recordings (Section 3.2) in glucose-free ECS (Fig. 4). Cells were pre-equilibrated for 25 min in ECS containing 3 mM glucose to minimise uncontrolled glycogen breakdown, then rinsed and

incubated for 5 min in glucose-free ECS. Thereafter, including agonist preparation and application, all solutions were glucose-free. Amplitudes were quantified over the final 100 s of each recording. Adenosine (100 nM) increased $[glucose]_i$ relative to vehicle (Δ 1.60 ± 0.21% vs 0.33 ± 0.09%; Mann-Whitney U = 41.5, p < 0.001). Selective A2B stimulation with BAY 60-6583 (1 µM) likewise elevated $[glucose]_i$ (Δ 1.13 ± 0.18% vs 0.27 ± 0.08%; U = 56, p < 0.001). Because these responses persist in the absence of extracellular glucose, they indicate mobilisation of intracellular glucose stores, rather than from increased glucose uptake, consistent with A2B-coupled glycogenolysis as the primary source of the adenosine-evoked $[glucose]_i$ rise.

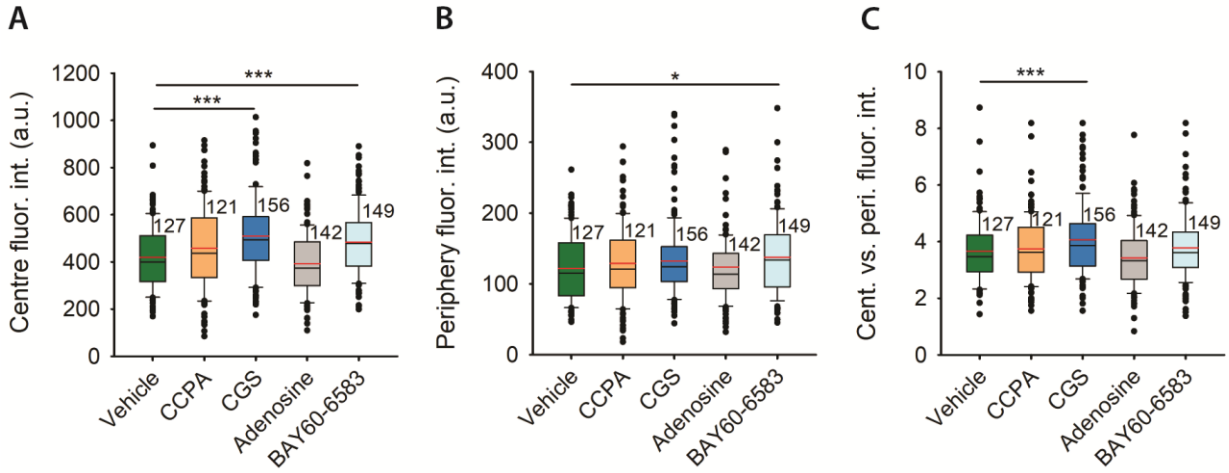

Figure 3. Adenosine receptor activation increases glycogen in astrocytes with distinct spatial patterns. Primary astrocytes were PAS-stained after 30 min pretreatment with vehicle (ECS), CCPA (100 nM; A1R), CGS21680 (100 nM; A2AR), adenosine (100 nM; non-selective), or BAY 60-6583 (1 µM; A2BR). Three square ROIs per cell were analysed along the short axis: perinuclear (ROI_1), middle (ROI_2) and peripheral (ROI_3); ROI_1 and ROI_3 are reported here. **(A)** Perinuclear PAS intensity (ROI_1). A2A and A2B stimulation increased glycogen relative to vehicle (Kruskal–Wallis H = 50.803, df = 4, p < 0.001; Dunn's: A2A > vehicle, A2B > vehicle, both p < 0.001). **(B)** Peripheral PAS intensity (ROI_3). Only A2B increased glycogen at the periphery (H = 11.243, df = 4, p = 0.024; Dunn's: A2B > vehicle, p < 0.05). **(C)** Perinuclear/periphery ratio (ROI_1/ROI_3). The ratio rose after A2A stimulation, indicating perinuclear-biased accumulation (H = 22.022, df = 4, p < 0.001; Dunn's: A2A > vehicle, p < 0.001). Data are mean ± SEM. n denotes independently analysed single cells.

Adenosine signalling decelerates glycogen turnover in astrocytes during recovery from starvation

To assess how adenosine receptors influence glycogen replenishment after nutrient stress, astrocytes were exposed to glucose-free ECS for 2 h ("starvation") and then allowed to recover for 2 h in ECS containing 3 mM glucose. PAS fluorescence was quantified (see Methods) in a.u. Glycogen was markedly reduced after starvation (n = 101) and rebounded with recovery (n = 132; Fig. 5D-F). In the perinuclear region, glycogen level increased by ~1.5-fold (from 292.0 ± 9.4 to 438.9 ± 14.4 a.u.; Kruskal–Wallis H = 279, df = 5, p < 0.001). In the peripheral cytoplasm, glycogen increased by ~1.4-fold (from 100.0 ± 3.8 to 143.8 ± 6.3 a.u.; H = 206.1, df = 5, p < 0.001). These consistent increases across compartments validate the recovery of glycogen stores, likely indicating their remodelling.

To test receptor-specific effects during recovery, parallel cultures received adenosine (100 nM; n = 89), CCPA (A1R, 100 nM; n = 168), CGS21680 (A2AR, 100 nM; n = 107), or BAY 60-6583 (A2BR, 1 µM; n = 52). As shown in Fig. 5A-C, adenosine and A2B stimulation significantly slowed glycogen replenishment in both compartments. Perinuclearly, glycogen fell by ~44% with adenosine and ~85% with A2B versus vehicle (vehicle 438.9 ± 14.4, adenosine 245.6 ± 18.0, BAY 60-6583 66.1 ± 2.4 a.u.; H = 279, df = 5, p < 0.001; Dunn's post hoc). In contrast, A2A stimulation increased perinuclear glycogen by ~16% (CGS21680 487.6 ± 16.5 a.u.; p < 0.001). In the periphery, only adenosine and A2B altered glycogen levels (H = 206.1, df = 5, p < 0.001): adenosine reduced recovery by ~45% (78.6 ± 6.0 vs 143.8 ± 6.3 a.u.), and A2B by ~90% (14.3 ± 0.8 a.u.). CCPA did not significantly alter absolute perinuclear or peripheral intensities compared with vehicle. Spatial profiling using the perinuclear/periphery ratio (ROI_1/ROI_3) showed a larger relative depletion at the periphery after receptor activation (vehicle 3.3 ± 0.09 vs A1 3.8 ± 0.09, A2A 4.0 ± 0.10, A2B 5.0 ± 0.20; H = 77.432, df = 5, p < 0.001; Dunn's). Thus, during recovery, adenosine and A2B signalling preferentially drain peripheral glycogen pools, whereas A2A favours perinuclear glycogen preservation/accumulation.

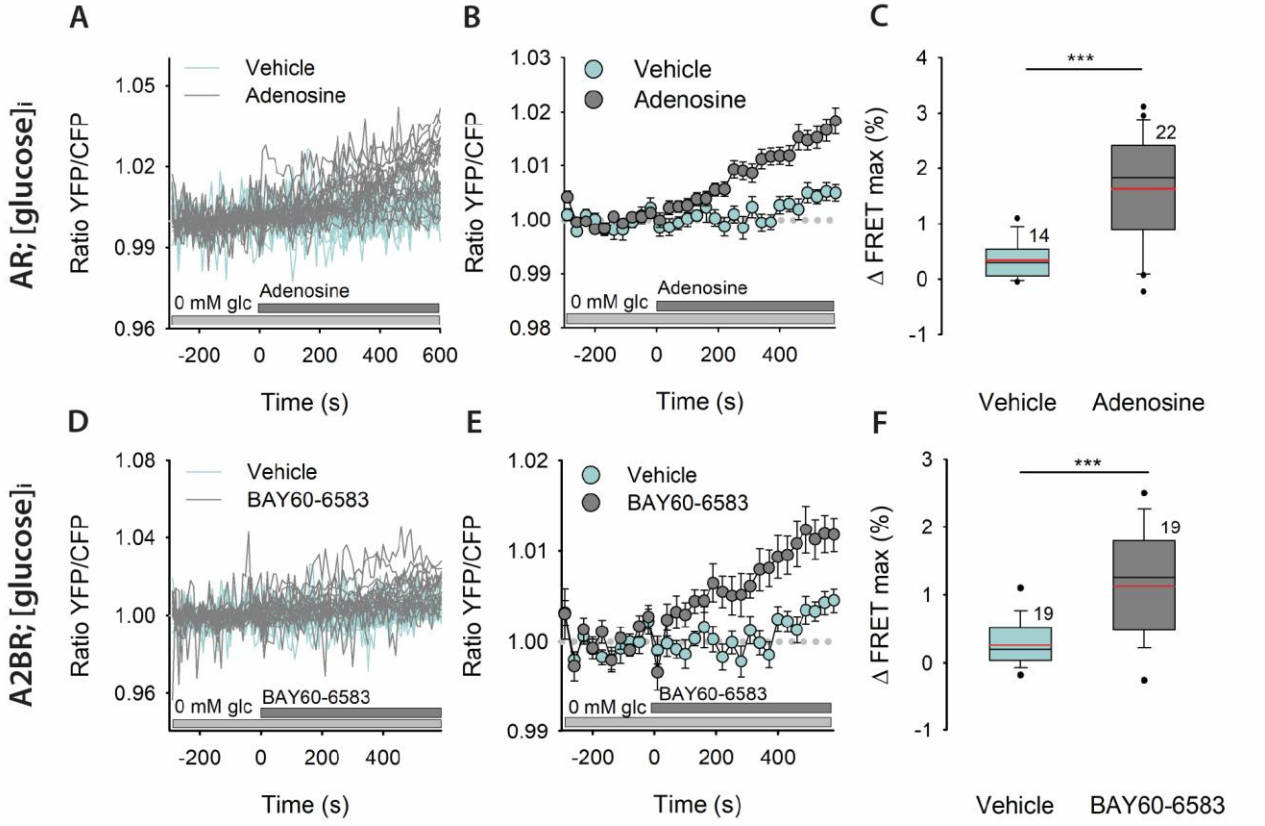

Figure 4. Adenosine receptor activation increases $[glucose]_i$ under glucose-free conditions. Astrocytes expressing FLII12Pglu-700μδ6 were pre-equilibrated for 25 min in ECS with 3 mM glucose, then 5 min in glucose-free ECS; all subsequent solutions (including agonists) were glucose-free. Cells were stimulated with adenosine (100 nM; **A, B, C**) or BAY 60-6583 (1 μM; A2B agonist; **D, E, F**); vehicle = glucose-free ECS. Time 0 marks the addition of the vehicle/agonist. The left panels (A, D) represent single-cell YFP/CFP ratio traces normalised to baseline (vehicle, blue; agonist, grey). The middle panels (**B, E**) represent mean ± SEM traces corresponding to the left panels, normalised baseline (=1). Increases in YFP/CFP reflect higher $[glucose]_i$. The right panels (**C, F**) represent summary amplitudes (mean ± SEM) computed over the final 100 s. Mann-Whitney U versus matched vehicle: adenosine ($U = 41.5$, $p < 0.001$), BAY 60-6583 ($U = 56.0$, $p < 0.001$). n denotes independently analysed single cells.

A2B activation increases astrocytic intracellular lactate

Intracellular lactate was monitored with the Laconic FRET nanosensor, reported as mTFP/Venus, where higher ratios indicate higher $[lactate]_i$ [63]. After a 300 s baseline, cells received adenosine (100 nM) or vehicle and were imaged for 600 s; 20 mM L-lactate was applied at the end to verify sensor responsiveness (data not shown). Imaging parameters matched the description in the Methods (2.4). Under these conditions, vehicle addition alone produced a 2.8 ± 0.6% increase in the FRET ratio (n = 22), and adenosine elicited a similar (2.7 ± 0.2%) increase (n = 16), with no significant difference between groups (Mann-Whitney U = 152; n.s., Fig. 6A-C). Furthermore, we measured $[lactate]_i$ following the addition of the A2B agonist, BAY 60-6583 (1 μM; Fig. 6D-F). In this setup, vehicle addition caused a rise of 2.0 ± 0.2% (n = 19), whereas BAY 60-6583 induced a larger increase of 3.4 ± 0.4% (n = 26; Mann-Whitney U = 137; p = 0.012).

Balanced receptor activation neutralises adenosine effects on cAMP

To probe second-messenger dynamics during adenosine receptor (AR) activation, we monitored intracellular cAMP with the Epac1-camps FRET nanosensor [64], reported as the CFP/YFP ratio so that an increase reflects higher $[cAMP]_i$ (Fig. 7). After a 300 s baseline, cells received adenosine (100 nM) or selective agonists and were imaged for 600 s; a 100 μM noradrenaline pulse verified sensor responsiveness at the end. For A1R, which couples to $G_i/_o$, cells were preincubated in 100 nM adenosine, and the A1 antagonist DPCPX (800 nM) was added at time 0 to relieve G_i inhibition. Unless noted, amplitudes were quantified in the last 5 s of the experiment indicated below. Adenosine (non-selective

AR activation) produced a 10.7 ± 1.3% rise in $[cAMP]_i$ (n = 20), not significantly different from vehicle (8.6 ± 1.1%, n = 24; Student's t(42) = -1.3, n.s.), quantified in the last 5 s. The vehicle increase is consistent with the preparation's known handling sensitivity, reducing the power to detect minor drug effects. A1R antagonism with DPCPX after adenosine preincubation elicited a transient $[cAMP]_i$ increase (9.0 ± 1.3%, n = 26) greater than vehicle (5.5 ± 1.1%, n = 25; Mann-Whitney U = 218, p = 0.045), measured 170 s after antagonist addition. This aligns with the relief of A1-mediated G_i tone. A2A receptor activation using CGS21680 (100 nM) produced a transient elevation in $[cAMP]_i$ (6.0 ± 0.9%, n = 26) versus vehicle (2.9 ± 0.5%, n = 19; U = 134, p = 0.01), quantified 195 s post-stimulation. A2B receptor activation using BAY 60-6583 (1 µM) induced a larger, sustained $[cAMP]_i$ increase (20.1 ± 2.4%, n = 24) relative to vehicle (13.1 ± 1.5%, n = 13; Student's t(35) = -2.7, p = 0.011), quantified 595 s post-stimulation.

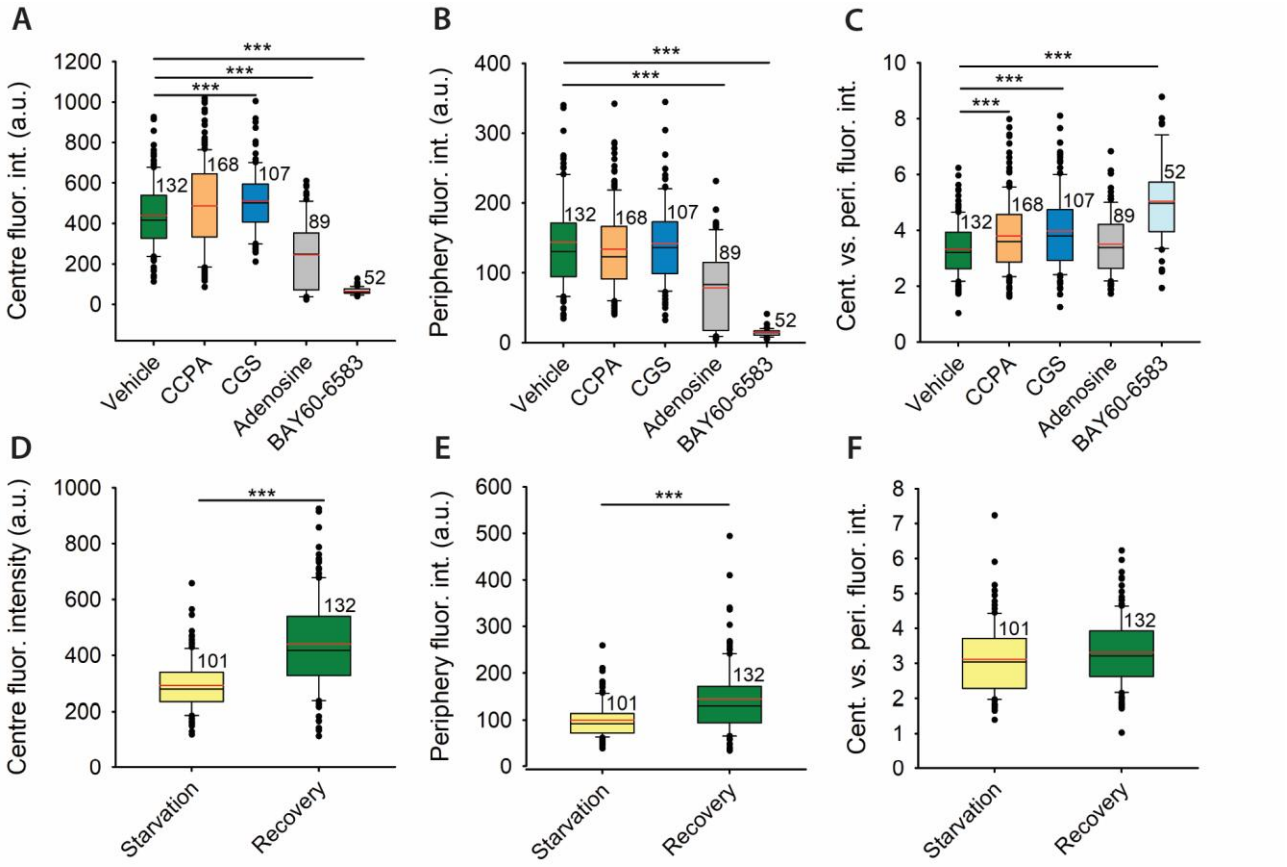

Figure 5. Adenosine receptor signalling modulates glycogen replenishment after glucose deprivation. Astrocytes were PAS-stained following glucose deprivation (starvation) and recovery. During recovery, cells received vehicle (ECS), CCPA (100 nM; A1R), CGS21680 (100 nM; A2AR), adenosine (100 nM; non-selective), or BAY 60-6583 (1 µM; A2BR). Panels A-C show agonist effects during recovery; panels D-F validate the paradigm by comparing starvation vs recovery in the vehicle. Three ROIs per cell were analysed along the short axis; perinuclear (ROI_1) and peripheral (ROI_3) are reported. **(A, D)** Perinuclear glycogen (ROI_1). A2B significantly reduced and A2A significantly increased glycogen versus vehicle; adenosine slowed recovery (all *p < 0.001). Kruskal–Wallis: H = 270.040, df = 5, p < 0.001; Dunn's post hoc as indicated in the main text. Panel D shows a higher ROI1 signal in recovery than in starvation. **(B, E)** Peripheral glycogen (ROI_3). A2B and adenosine significantly reduced glycogen versus vehicle (*p < 0.001), whereas A2A did not differ from vehicle. Kruskal–Wallis: H = 206.124, df = 5, p < 0.001. Panel E shows a higher ROI_3 signal in recovery vs starvation. **(C, F)** Perinuclear/periphery ratio (ROI_1/ROI_3). The ratio increased after A1, A2A, and A2B stimulation, indicating greater peripheral depletion than in perinuclear regions. Kruskal–Wallis: H = 77.432, df = 5, p < 0.001; Dunn's post hoc test significant versus vehicle. Data are mean ± SEM; n denotes independently analysed single cells.

The absence of a net adenosine effect likely reflects balanced co-activation of A1 (G_i) with A2A/A2B (G_s/Gq) pathways, yielding opposing influences on adenylyl cyclase. Vehicle-evoked increases further narrow the detectable drug-vehicle difference. In contrast, disinhibiting A1 or selectively engaging A2A/A2B reveals clear cAMP elevations, with A2B producing the most sustained response. This is consistent with its

prominent role in driving acute glycogen breakdown and the associated increase in $[glucose]_i$.

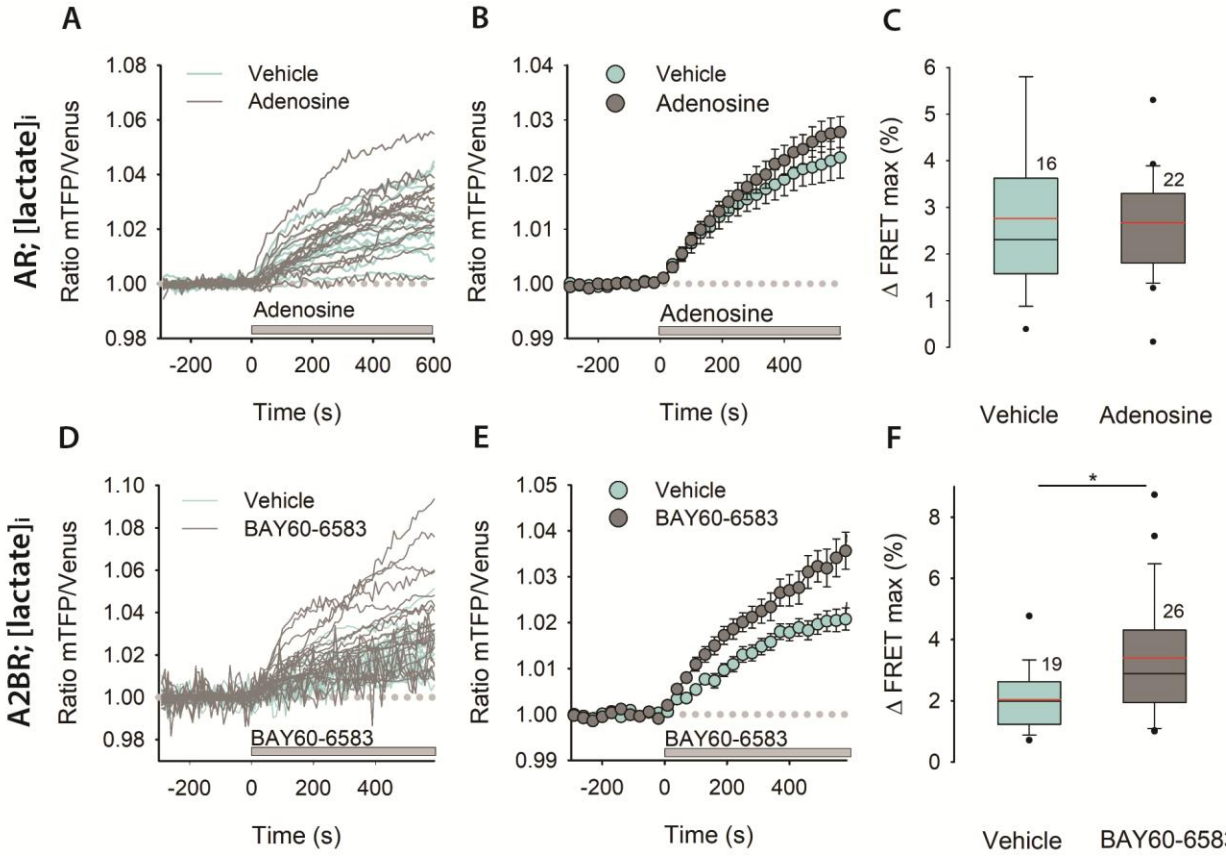

Figure 6. $[lactate]_i$ dynamics after adenosine or vehicle addition. Astrocytes expressing Laconic were imaged after a 300 s baseline, then stimulated with vehicle (ECS; blue) or agonist solution (grey; 100 nM adenosine in panels **A-C** or 1 µM BAY 60-6583 in panels **D-F**); time 0 marks addition. The left panels (**A, D**) represent single-cell mTFP/Venus ratio traces normalised to baseline (each line represents one cell). The middle panels (B, E) represent mean ± SEM traces corresponding to the left panels. Changes in $[lactate]_i$ were quantified over the final 100 s of the recording. The right panels **(C, F)** represent summary amplitudes (mean ± SEM). No significant difference was detected between vehicle and 100 nM adenosine addition (A-C; Mann-Whitney U = 152, p = 0.487). Sample sizes: vehicle n = 22, adenosine n = 16. Selective activation of A2B adenosine receptor shows a significant increase in $[lactate]_i$ after the addition of 1 µM BAY 60-6583 (**D-F**; Mann-Whitney U = 137, p = 0.012), indicating that A2B signalling can promote glycolytic lactate production. Sample sizes: vehicle n = 19, BAY 60-6583 n = 26. A 20 mM L-lactate pulse at the end verified sensor responsiveness (not shown). n denotes independently analysed single cells.

Adenosine receptor subtype specific $[Ca^{2+}]_i$ responses: transient (A1, adenosine) vs sustained (A2)

To examine Ca^{2+} dynamics during adenosine receptor (AR) activation, we loaded astrocytes with CAL520-AM and imaged changes in fluorescence (a.u.) (Fig. 8). Cells received adenosine (100 nM), CCPA (100 nM; A1R), CGS21680 (100 nM; A2AR), BAY 60-6583 (1 µM; A2BR), or vehicle after a 300 s baseline. Each experiment included its own vehicle control; pooled vehicle data are shown in Fig. 8A (blue), and per-experiment vehicle traces are displayed in panels E, I and M in a lighter shade. Two analysis windows were used: (i) a terminal window (right panel) defined as the last 10 frames (30 s) at 10 min post-stimulation, and (ii) a peak window (second-to-the-right panel) capturing the maximal 30 s increase (A2A at ~60 s; A2B at ~90 s). Group comparisons used the Mann-Whitney U test. Adenosine (all ARs) activation produced a transient rise at 30 s (28.8 ± 8.9 a.u.; n = 19) versus vehicle (12.7 ± 3.1 a.u.; n = 76; U = 472, p = 0.020). A1R stimulation likewise yielded a transient increase (55.1 ± 11.7 a.u.; n = 23). By the end of the experiment (terminal window), amplitudes were not significantly different from vehicle (vehicle: 31.3 ± 2.2 a.u.; adenosine: 38.0 ± 8.9 a.u.; A1R: 33.4 ± 3.8 a.u.). In contrast, A2A and A2B agonists produced sustained $[Ca^{2+}]_i$ elevations at the terminal window: A2A, 46.8 ± 3.9 a.u. (n = 43) and A2B, 41.7 ± 4.5 a.u. (n = 24) versus vehicle, 31.3 ± 2.8 a.u. (A2A: U = 930, p < 0.001; A2B: U = 624, p = 0.020). Peak responses were also significantly larger than vehicle:

A2A, 36.5 ± 5.4 a.u. at ~60 s vs 15.1 ± 2.6 a.u. (U = 846, $p \leq 0.001$); A2B, 59.7 ± 11.1 a.u. at ~90 s vs 19.7 ± 3.3 a.u. (U = 496, $p \leq 0.001$). Taken together, adenosine and A1R activation evoke transient $[Ca^{2+}]_i$ increases that decrease in 10 min, whereas A2A and A2B drive more persistent elevations, consistent with prolonged second-messenger engagement by A2 signalling.

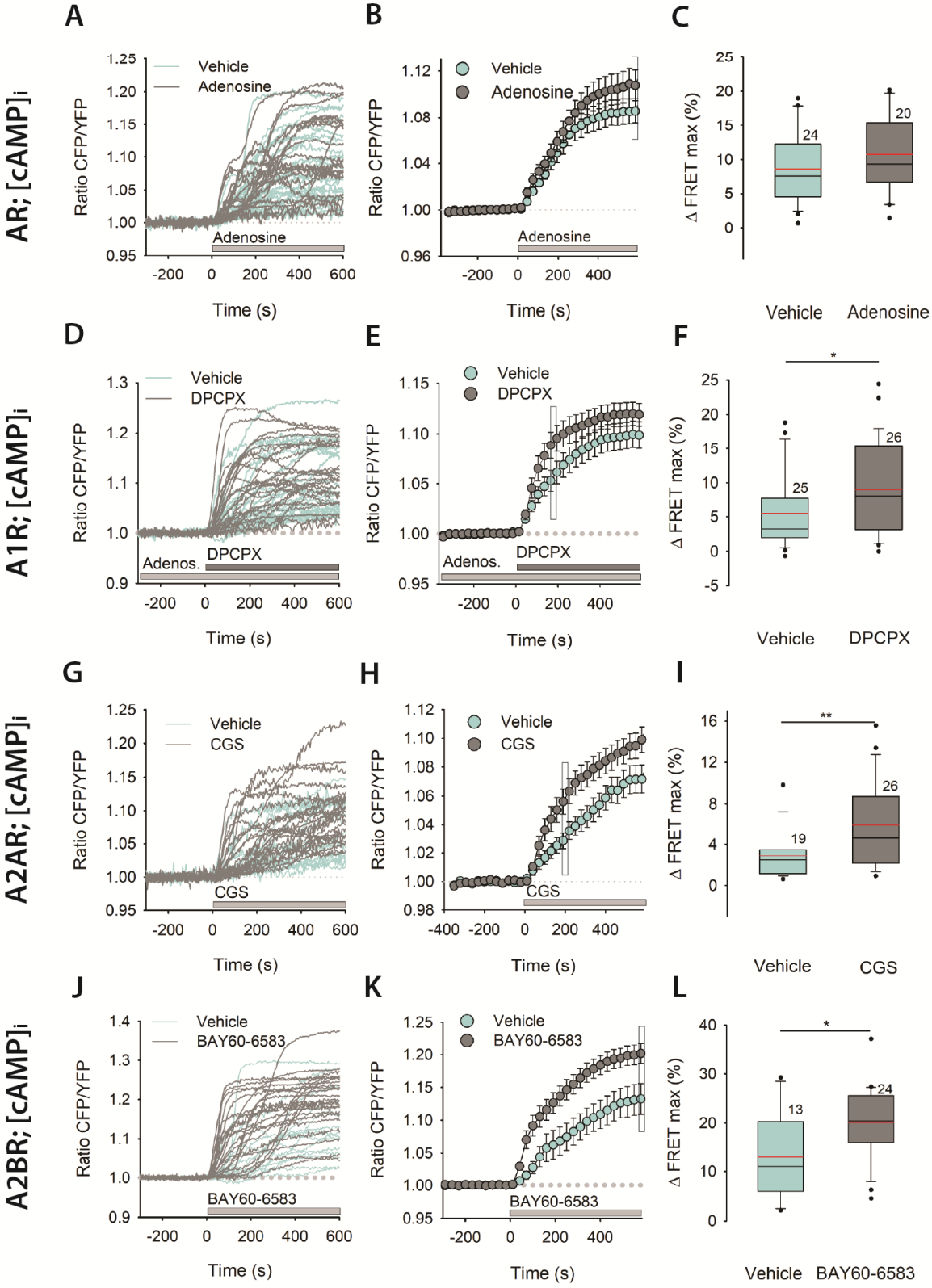

Figure 7. Adenosine receptor-dependent cAMP dynamics in astrocytes. Astrocytes expressing Epac1-camps were imaged after a 300 s baseline and then received vehicle (ECS) or the indicated (ant)agonist; a 100 µM noradrenaline pulse at the end verified sensor responsiveness (not shown). $[cAMP]_i$ is reported as the CFP/YFP ratio. The left panels (**A, D, G, J**) represent single-cell CFP/YFP ratio traces normalised to baseline (each line: one cell, vehicle, blue; (ant)agonist, grey). The middle panels (B, E, H, K) represent mean ± SEM normalised traces. The right panels (**C, F, I, L**) represent summary amplitudes (mean ± SEM) calculated within the square-marked 5 s window (panel-specific below). Rectangles in panels B, E, H, and K mark the 5-s analysis windows used to compute the amplitudes in panels C, F, I, and L; for each condition, the window was positioned at the time point of maximal divergence between the agonist and its matched vehicle trace, so the rectangles occur at different times across panels. n denotes independently analysed single cells. **(A-C)** Non-selective activation (adenosine, 100 nM). Vehicle n = 24, adenosine n = 20; window = final 5 s. No significant difference (Student's $t(42) = -1.3$, $p = 0.212$), consistent with balanced co-activation of inhibitory (A1) and stimulatory (A2) pathways. **(D-F)** A1 antagonism after adenosine preincubation. Cells were preincubated in adenosine (100 nM); at time 0, DPCPX (800 nM) or vehicle was added. Vehicle n = 25, DPCPX n = 26; window = 170 s post-addition. DPCPX > vehicle (Mann-Whitney $U = 218$, $p = 0.045$), indicating relief of A1-mediated G_i inhibition. **(G-I)** A2A activation (CGS21680, 100 nM). Vehicle n = 19, CGS21680 n = 26; window = 195 s. CGS21680 > vehicle ($U = 134$, $p = 0.01$), yielding a transient $[cAMP]_i$ rise. (J-L) A2B activation (BAY 60-6583, 1 µM). Vehicle n = 13, BAY 60-6583 n = 24; window = 595 s. BAY 60-6583 > vehicle (Student's $t = -2.669$, $p = 0.011$, $df = 35$), producing a larger, sustained increase in $[cAMP]_i$. n denotes independently analysed single cells.

A2B receptor antagonism attenuates the effect of 100 nM adenosine on intracellular glucose levels

To test whether the increase in intracellular glucose evoked by 100 nM adenosine is mediated by A2B receptors, we performed pharmacological blockade experiments in cultured astrocytes. Cells were preincubated with the selective A2B receptor antagonist PSB-603 (10 µM), while control cells were exposed to vehicle (ECS) only. Following preincubation, 100 nM adenosine was applied to both conditions, and intracellular glucose was monitored using the same glucose sensor and analysis pipeline as in the initial adenosine experiments (Section 3.2). Glucose signals were normalised to baseline. In vehicle-treated cells, 100 nM adenosine reliably reproduced the previously observed increase in intracellular glucose (1.77 ± 0.25%, Section 3.2, Fig. 2). As these responses were indistinguishable from the original dataset, the vehicle data were pooled with the corresponding measurements from Section 3.2. In contrast, PSB-603 markedly attenuated the adenosine-evoked glucose rise: in antagonist-treated cells, adenosine induced only a 0.31 ± 0.25% change (Fig. 9). This reduction was statistically significant compared with adenosine alone (Mann–Whitney U test: $U = 78$, $p < 0.001$). Together, these results indicate that the dynamic increase in intracellular glucose triggered by 100 nM adenosine is strongly A2B receptor–dependent, with A2B antagonism largely abolishing the response.

Inhibition of equilibrative nucleoside transporters does not abolish the adenosine-evoked intracellular glucose response

To test whether adenosine uptake and downstream AMP/AMPK signalling contribute to adenosine-evoked changes in intracellular glucose, we inhibited equilibrative nucleoside transporters (ENTs) using dipyridamole (10 µM). After preincubation, astrocytes were exposed to dipyridamole alone, dipyridamole + 100 nM adenosine, or dipyridamole + 1 µM BAY 60-6583. Intracellular glucose was recorded using the same protocol as in earlier experiments and normalised to the final 100 s of baseline. Because dipyridamole exhibits intrinsic fluorescence, an apparent bleaching component was observed (grey blocks in Fig. 10) and was excluded from interpretation. The fluorescence slope at the beginning of the recording and following stimulus addition (stimuli were also prepared in dipyridamole-containing ECS) remained comparable, indicating a consistent dye-related trend rather than a stimulus-dependent artefact. Therefore, responses were quantified as the peak-to-trough change in FRET ratio (ΔFRET; max–min) (Figure 10 C, F). Dipyridamole alone produced a modest ΔFRET (1.71 ± 0.27%), which served as the baseline control under ENT-inhibited conditions. In contrast, in the continued presence of dipyridamole, 100 nM adenosine elicited a pronounced increase in intracellular glucose (6.07 ± 0.50%). Likewise, 1 µM BAY 60-6583 in dipyridamole induced a similarly robust increase (6.01 ± 0.31%). Both responses were consistently larger than the dipyridamole-alone condition and differed significantly by one-way ANOVA ($F = 39.19$, $df = 2$; $p < 0.001$) with Holm–Šídák post hoc tests ($t_{\text{vehicle vs adenosine}} = 8.24$, $t_{\text{vehicle vs BAY 60-6583}} = 7.44$). Thus, blocking ENT-mediated uptake did not abolish the glucose response to adenosine; instead, the response was preserved under these conditions. Together with the PSB-603 experiments, these findings support the conclusion that the effect of 100 nM adenosine on astrocytic intracellular glucose is predominantly mediated by extracellular receptor signalling, specifically via A2B receptors, rather than by intracellular adenosine uptake and metabolism through ENTs and AMPK.

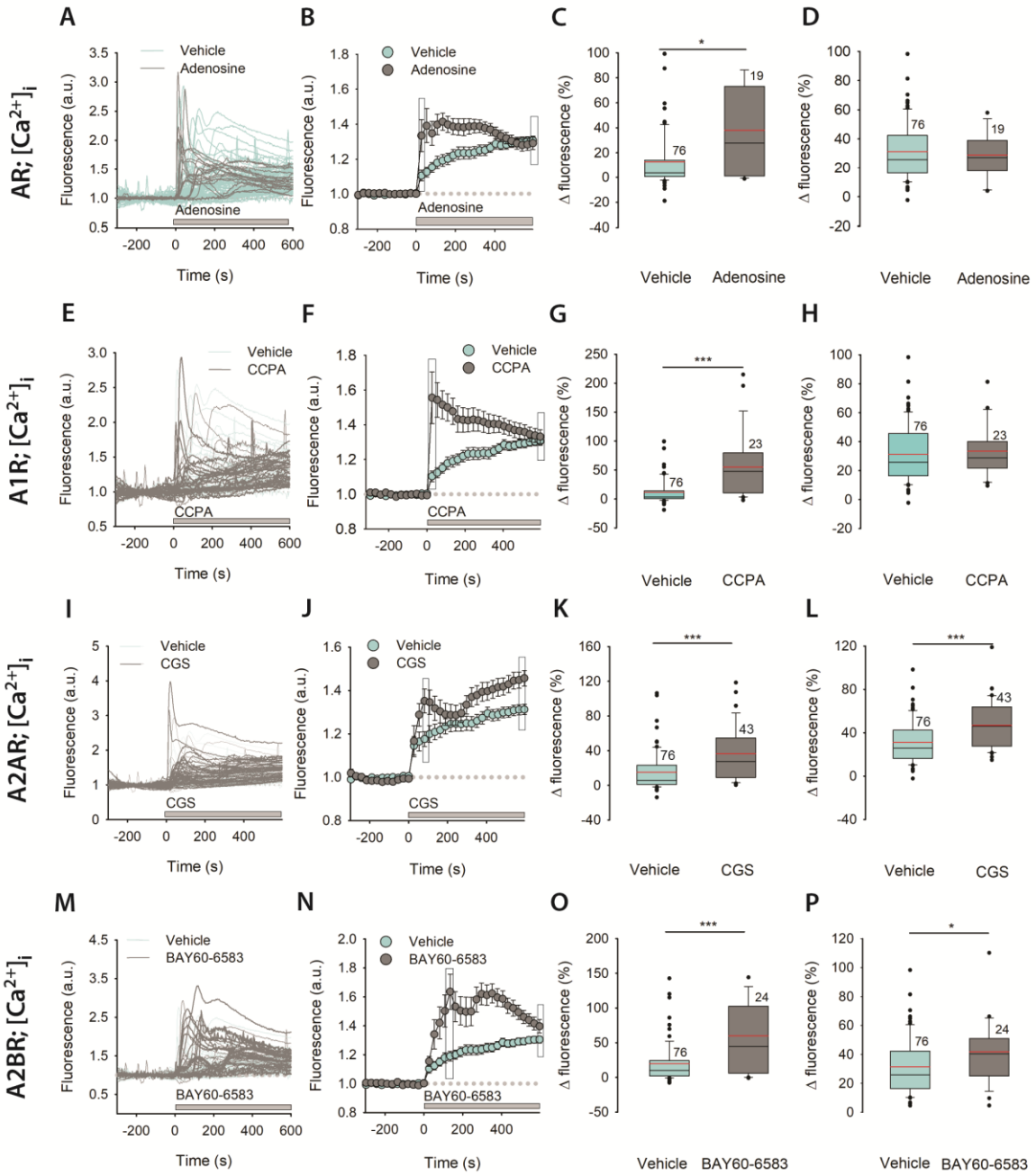

Figure 8. Adenosine receptor-dependent $[Ca^{2+}]_i$ dynamics in astrocytes. Astrocytes loaded with CAL520-AM were imaged after a 300 s baseline and then received vehicle (ECS; blue) or the indicated agonist (grey). Traces are normalised to baseline fluorescence and reported as arbitrary units (a.u.). The left panels **(A, E, I, M)** represent single-cell normalised traces (each line: one cell). The second-to-the-left panels **(B, F, J, N)** represent mean ± SEM normalised time courses. The second-to-the-right panels **(C, G, K, O)** show peak window amplitudes (mean ± SEM) quantified over 30 s at the indicated post-stimulus time. The right panels **(D, H, L, P)** show terminal window amplitudes (mean ± SEM) quantified over the last 30 s at 10 min. Square boxes on mean ± SEM normalised time courses (B, F, J, N) mark analysis windows. **(A-D)** Adenosine, 100 nM (non-selective). Vehicle n = 76, adenosine n = 19. Peak (30-60 s): adenosine > vehicle (U = 472, p = 0.020). Terminal: no significant difference (n.s.; not shown). **(E-H)** A1 activation, CCPA 100 nM. Vehicle n = 76, CCPA n = 23. Peak (30-60 s): CCPA > vehicle (U = 316, p < 0.001). Terminal: n.s. (I-L) A2A activation, CGS21680 100 nM. Vehicle n = 76, CGS21680 n = 43. Peak (~60 s): CGS21680 > vehicle (U = 846, p < 0.001). Terminal (10 min): CGS21680 > vehicle (U = 930, p < 0.001), indicating a sustained elevation. **(M-P)** A2B activation, BAY 60-6583 1 µM. Vehicle n = 76, BAY 60-6583 n = 24. Peak (~90 s): BAY 60-6583 > vehicle (U = 496, p < 0.001). Terminal (10 min): BAY 60-6583 > vehicle (U = 624, p = 0.020), consistent with a sustained response. All statistics: Mann-Whitney U tests (two-tailed). n denotes independently analysed single cells.

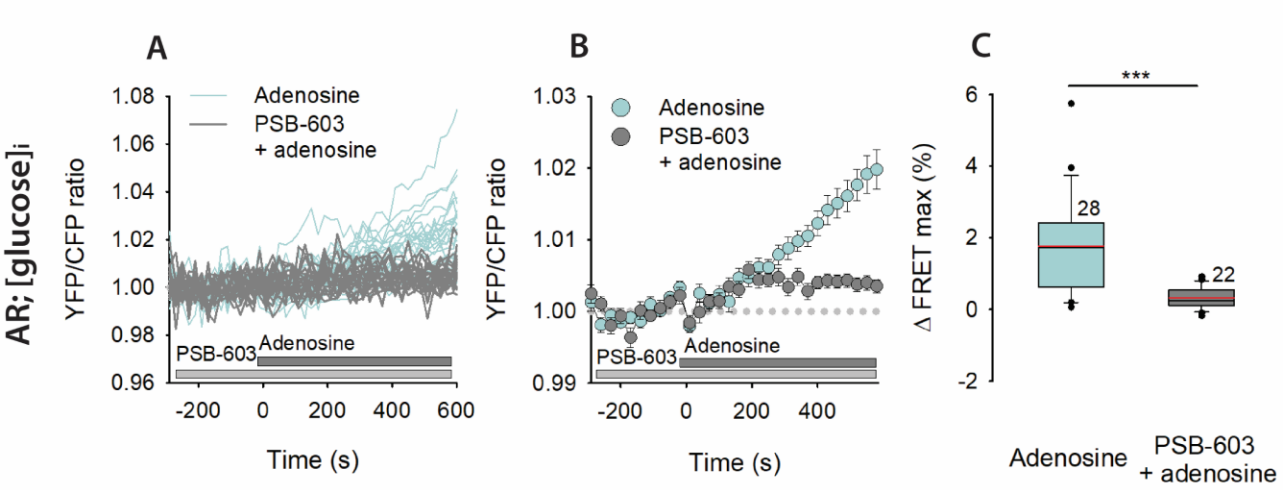

Figure 9. A2B receptor antagonism attenuates the 100 nM adenosine–evoked increase in intracellular glucose. Astrocytes expressing FLII12Pglu-700μδ6 were preincubated with the selective A2B antagonist PSB-603 (10 μM; grey) or vehicle (ECS; blue) and then stimulated with adenosine (100 nM). Time 0 marks adenosine application. **(A)** Representative single-cell YFP/CFP ratio traces, baseline-normalised. **(B)** Corresponding mean ± SEM traces. (C) Summary response amplitudes (mean ± SEM), quantified over the final 100 s of the recording. An increase in YFP/CFP indicates higher $[glucose]_i$. Adenosine alone increased $[glucose]_i$ (1.77 ± 0.25%), whereas PSB-603 markedly reduced the response (0.31 ± 0.25%; Mann–Whitney U = 78, $p < 0.001$). n indicates independently analysed single cells.

DISCUSSION

Astrocytes integrate metabolic and signalling demands by coupling extracellular cues to intracellular energy handling. Building on prior work implicating adenosine in sleep pressure, gliotransmission, and brain energy balance [1-4], our single-cell readouts show that receptor-specific adenosine signalling reshapes glucose availability, glycogen distribution and turnover, and second-messenger dynamics in cultured astrocytes.

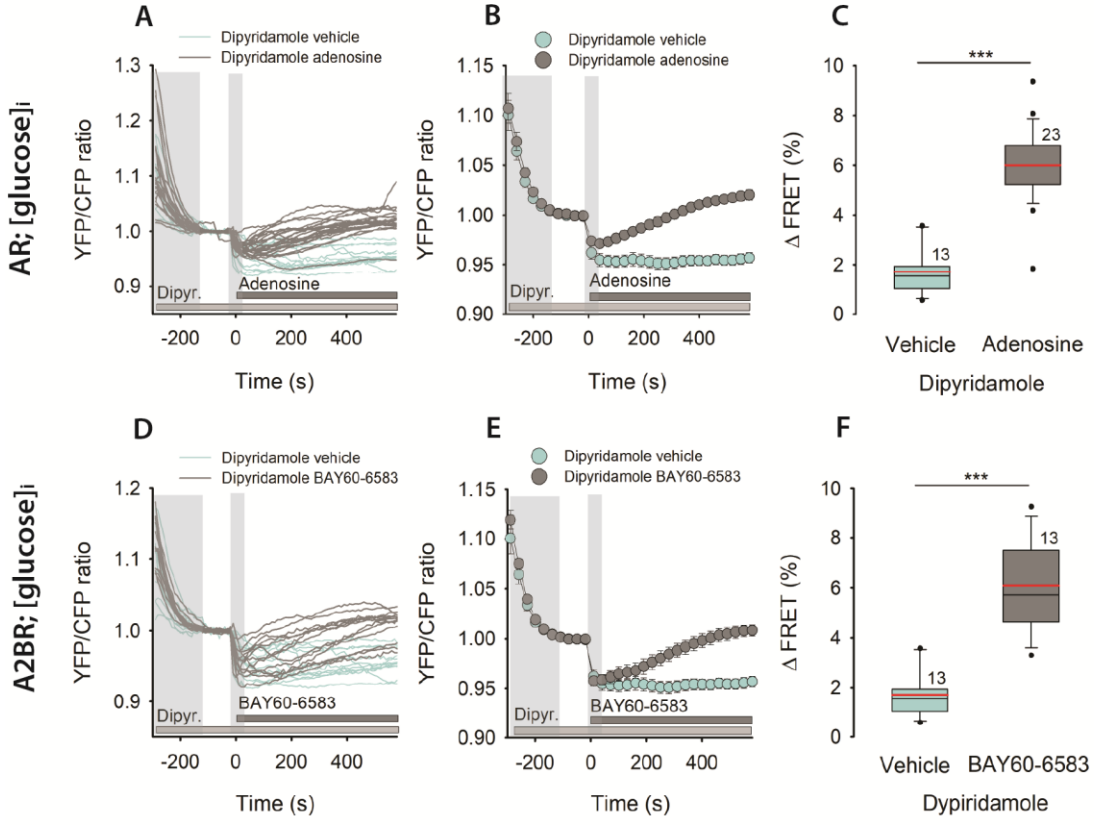

Figure 10. ENT inhibition preserves the adenosine-evoked intracellular glucose response. Astrocytes expressing FLII12Pglu-700μδ6 were preincubated with the ENT inhibitor dipyridamole (10 μM) and then stimulated with adenosine (100 nM; grey A–C), BAY 60-6583 (1 μM; A2B agonist; grey D–F), or dipyridamole alone (vehicle; blue). Time 0 marks agonist/vehicle application. **(A, D)** Representative single-cell YFP/CFP ratio traces, normalised to the final 100 s of baseline. **(B, E)** Corresponding mean ± SEM traces. Grey blocks indicate periods affected by dipyridamole intrinsic fluorescence and were excluded from interpretation/quantification. **(C, F)** Summary amplitudes quantified as peak-to-trough ΔFRET (max–min). Increases in YFP/CFP indicate higher $[glucose]_i$. Dipyridamole alone produced a small increase in $[glucose]_i$ (1.71 ± 0.27%), whereas dipyridamole + adenosine and dipyridamole + BAY 60-6583 evoked larger increases (6.07 ± 0.50% and 6.01 ± 0.31%, respectively). n indicates independently analysed single cells.

Astrocytic glycogen is a rapid, locally deployable energy reserve that yields glucose and lactate, and adenosine receptors modulate its mobilisation [38]. Adenosine accumulates during high metabolic load, contributes to sleep pressure, and may couple astrocyte metabolism to behavioural state [32]. Recent work indicates that adenosine receptor signalling shapes cAMP and Ca^{2+} dynamics that drive glycogenolysis and lactate production, yet receptor-specific mechanisms in astrocytes remain incompletely defined [37]. Here, we used ligand-specific concentrations to approximate EC_{80} for each receptor in astrocytes, guided by IUPHAR values and prior cell-based assays, to delineate how A1, A2A, and A2B receptors regulate astrocytic energy handling, quantifying adenosine-dependent changes in intracellular glucose and glycogen, lactate dynamics, and the underlying second messengers (cAMP, Ca^{2+}). In this study, we focused on A1, A2A and A2B receptors because their expression and pharmacology in rodent astrocytes are relatively well established, and selective ligands are available. By contrast, pharmacological tools for A3 receptors in this preparation are less selective, and current evidence for a defined role of A3 in astrocyte glycogen metabolism is limited; we therefore did not include A3 activation in the present analysis.

Among adenosine receptor subtypes, A2B has been linked most directly to stimulation of glucose consumption, glycolysis, and lactate release via cAMP-PKA signalling [37]. Our observation that adenosine and an A2B agonist elevate $[glucose]_i$ even in the absence of extracellular glucose argues for glycogen breakdown as the primary source of glucose. The slightly smaller A2B effect in glucose-free medium compared with control suggests that simultaneous uptake (present at 3 mM glucose) usually contributes to the net $[glucose]_i$ rise. That A2A agonist did not acutely raise $[glucose]_i$ under our conditions supports a more indirect role for A2A in astrocyte energy metabolism [6, 41, 42] despite evidence for its expression in astrocytes [61, 62]; but see [37] for RNA-seq. Our study does not aim to resolve this controversy but instead uses modest A2A immunoreactivity together with consistent pharmacological effects as evidence that A2A-coupled signalling is present in our preparation. Functionally, this aligns with A2A modulating energetically costly processes (e.g., glutamate uptake), while A2B more directly mobilises intracellular glucose pools.

PAS mapping of glycogen stores resolved regional differences. A2A increased perinuclear stores, whereas A2B increased both perinuclear and peripheral glycogen. Upon recovery from glucose deprivation, adenosine and A2B decreased replenishment in both regions, consistent with ongoing mobilisation; conversely, A2A enhanced perinuclear glycogen replenishment. The preferential peripheral depletion under several conditions suggests compartmentalised turnover near astrocyte processes that interface with synapses and vessels [65]. One mechanistic interpretation is that A2B signalling draws on peripheral glycogen to meet rapid local demands (e.g., ion and transmitter clearance), while A2A signalling biases storage near the soma, where glycogen synthase and related enzymes may be scaffolded.

Although A2B receptors are typically described as low-affinity (micromolar) adenosine receptors, our data indicate that the intracellular glucose response to 100 nM adenosine in astrocytes is predominantly A2B-driven. This interpretation is supported by three observations: adenosine and the A2B agonist BAY 60-6583 evoke highly similar $[glucose]_i$ responses; both responses persist without extracellular glucose, indicating an intracellular glycogen source; and A2B stimulation alters glycogen content/redistribution and activates cAMP signalling, consistent with a cAMP/PKA-linked glycogenolytic programme. Accordingly, we treated adenosine as a non-selective stimulus and used subtype-selective pharmacology to identify the pathway mediating its net metabolic effect, combining A2B antagonism with blockade of equilibrative nucleoside transporters. Two findings clarify the mechanism. First, PSB-603 strongly attenuated the 100 nM adenosine-evoked increase in glucose, indicating that A2B receptors are required and consistent with the BAY 60-6583 phenotype. Second, ENT inhibition with dipyridamole did not abolish the response: adenosine (and BAY 60-6583) still produced robust increases in $[glucose]_i$, arguing against a dominant role for intracellular uptake and AMP/AMPK signalling at this concentration.

Collectively, the loss of effect with A2B antagonism and preservation under ENT blockade supports a model in which 100 nM adenosine acts primarily via astrocytic

A2B receptors to engage cAMP–PKA signalling, drive glycogenolysis, and elevate intracellular glucose.

The A2B-dependent rise in $[glucose]_i$ under glucose-free conditions, together with slowed replenishment during recovery, fits a sequence in which adenosine couples high ATP demand to rapid glycogen mobilisation followed by delayed resynthesis, a pattern relevant for sleep pressure, plasticity, and ANLS-guided fuel shuttling [1, 32, 37]. Sustained A2A/A2B-evoked Ca^{2+} signals may boost energy-demanding transporter activity (e.g., GLT-1, Na^+/K^+-ATPase) and endfoot functions at blood vessels, thereby shaping local metabolite availability. By contrast, the balanced cAMP response to adenosine may reflect the co-activation of inhibitory (A1, G_i) and stimulatory (A2, G_s/Gq) arms, providing a homeostatic brake when extracellular adenosine rises broadly during prolonged wake.

Beyond physiological sleep–wake regulation, adenosine- and glycogen-dependent astrocyte metabolism is likely to be engaged under pathological conditions characterised by chronic metabolic stress [22]. In neurodegenerative disorders, such as Alzheimer's disease, early loss of noradrenergic neurons in the *locus coeruleus* and fragmentation of sleep–wake cycles are associated with altered extracellular adenosine signalling and impaired network resilience [6]. In such settings, receptor-specific control of astrocyte glycogen may influence whether astrocytic energy reserves buffer neuronal stress or become progressively depleted.

Although adenosine is often associated with enhanced glycolysis and lactate release [37], vehicle addition alone increased the Laconic ratio in our setup, and adenosine-stimulated changes were not significantly different from vehicle. Given the known mechanosensitivity of astrocytes to fluid handling, these conditions could partly obscure receptor-dependent lactate effects [66].

In contrast, selective A2B activation with BAY 60-6583 produced a significantly larger increase in $[lactate]_i$ compared with vehicle, indicating that A2B signalling can promote glycolytic lactate production at the single-cell level. This effect is compatible with A2B-evoked glucose mobilisation predominantly reflecting glycogenolysis, because pool size changes in $[glucose]_i$ and flux (lactate production/release) operate on different timescales and can be at least transiently uncoupled.

The cAMP data fit classical coupling: A1 ($G_i/_o$) inhibits adenylyl cyclase, so A1 antagonism after adenosine preincubation disinhibits cAMP; A2A (G_s) and A2B (G_s/G_q) elevate cAMP, with A2B producing the most sustained rise [67-69]. The absence of a net effect of adenosine likely reflects balanced co-activation of A1 and A2 receptors plus the slight vehicle-evoked increase. For Ca^{2+}, adenosine and A1 yielded transient increases, consistent with Gβγ-PLCβ-IP_3 pathways [70, 71], whereas A2A/A2B produced sustained elevations. Prior work attributes A2A-evoked Ca^{2+} increases to PKA-dependent mechanisms that are independent of canonical PLC/IP_3 or RyR signalling [72-74]; A2B may recruit both Gs-cAMP/PKA and Gq-PLCβ/IP_3 arms [67-69], rationalising its sustained Ca^{2+} profile here. Differences in cAMP and Ca^{2+} signalling account for the contrasting metabolic results. These observations suggest that receptor-specific combinations of cAMP and Ca^{2+} signalling contribute to the tuning of astrocyte glycogen metabolism. Although we did not directly inhibit PKA or chelate intracellular Ca^{2+} in the present work, the convergence of receptor-specific signalling and metabolic phenotypes supports the view that adenosine receptor–specific combinations of cAMP and Ca^{2+} signals coordinate the balance between glycogen mobilisation and replenishment in astrocytes and should be an essential target for future mechanistic dissection.

Downstream effectors such as glycogen synthase kinase-3β (GSK3β), a constitutively active serine/threonine kinase that phosphorylates and inhibits glycogen synthase, thereby restraining glycogen synthesis [75], are likely to contribute to the coupling between A2B receptor activation and glycogen metabolism. Directly probing A2B-dependent regulation of GSK3β phosphorylation state will therefore be an important target for future studies.

The small $[glucose]_i$ increase with high-dose CCPA likely reflects reduced selectivity or crosstalk. Notably, A1-A2A heteromers can behave as adenosine concentration sensors, where A2A occupancy limits A1-G_i coupling [72]. Such functional antagonism provides a mechanistic basis for dose-dependent and context-dependent outputs and may contribute to the balanced net effects of adenosine. Functionally, astrocytes respond to A2A activation; however, reports of astrocytic A2A expression remain mixed [6, 37, 40, 41, 61, 62].

With advancing age, the brain increasingly experiences chronic low-grade metabolic and inflammatory stress, alongside progressive disruption of sleep–wake architecture and neuromodulatory tone [22, 36, 43]. These age-related changes are associated with altered extracellular adenosine signalling and with transcriptional and functional remodelling of astrocytes, including their metabolic pathways [3, 6, 71]. In this context, the receptor-specific balance that we describe here may become a critical determinant of whether astrocyte glycogen acts as a resilient energy buffer or instead becomes chronically depleted in the aging brain. Our data thus provide a framework for future *in vivo* studies testing how age-dependent changes in adenosine receptor expression or signalling bias astrocyte glycogen metabolism.

Future studies in acute brain slices and *in vivo*, as well as under defined physiological and pathological states, will be required to determine how the receptor-specific roles identified here translate to intact neural circuits.

Conclusions

A2B signalling emerges as a central regulator of glycogenolysis that acutely mobilises glucose (via glycogenolysis) and slows the glycogen store replenishment during recovery, while A2A preferentially builds perinuclear glycogen. The distinct cAMP/Ca^{2+} fingerprints, balanced for adenosine, transient for A1, and sustained for A2A/A2B, provide a mechanistic framework linking adenosine to state-dependent astrocyte energy management. Data indicate that adenosine elevates astrocytic intracellular glucose primarily via A2B receptor signalling. Receptor-specific pathways help explain how astrocytes tune local fuel availability and may highlight adenosine's roles in sleep homeostasis, plasticity, behaviour, and potentially in age- and disease-related disruptions of brain energy homeostasis.

Acknowledgements

This work was supported by grants from the Slovenian Research and Innovation Agency (grant nos. P3-310, J3-50104, J7-3153, J3-2523, J4-60077, I0-0034 Celica, I0-0048 Cipkebip, I0-0022 UL), EU Interreg Italia-Slovenia Immunocluster-2, and Coherence. The authors gratefully acknowledge Dr. Katja Fink for her valuable assistance with the experimental work.

Conflicts of Interest

The authors declare no conflicts of interest.

Data Availability Statement

The datasets generated and analysed in this study, including raw and processed FRET traces (glucose, lactate, cAMP), Ca^{2+} imaging data, and original microscopy image files (FRET images and PAS-stained images), are available from the corresponding author upon reasonable request.

Supplementary Materials

The Supplementary data are available online at: www.aginganddisease.org/EN/10.14336/AD.2025.1389.

References

[1] Alberini CM, Cruz E, Descalzi G, Bessières B, Gao V (2018). Astrocyte glycogen and lactate: New insights into learning and memory mechanisms. Glia, 66:1244–1262.

[2] Kreft M, Bak LK, Waagepetersen HS, Schousboe A (2012). Aspects of astrocyte energy metabolism, amino acid neurotransmitter homoeostasis and metabolic compartmentation. ASN Neuro, 4:AN20120007.

[3] Verkhratsky A, Nedergaard M (2018). Physiology of astroglia. Physiol Rev, 98:239–389.

[4] Zhang Y, Barres BA (2010). Astrocyte heterogeneity: an underappreciated topic in neurobiology. Curr Opin Neurobiol, 20:588–594.

[5] Lemos C, Pinheiro BS, Beleza RO, Marques JM, Rodrigues RJ, Cunha RA, et al. (2015). Adenosine A2B receptor activation stimulates glucose uptake in the mouse forebrain. Purinergic Signal, 11:561–569.

[6] Lopes CR, Cunha RA, Agostinho P (2021). Astrocytes and adenosine A2 A receptors: Active players in Alzheimer's disease. Front Neurosci, 15:666710.

[7] Zhu Y, Ma J, Li Y, Gu M, Feng X, Shao Y, et al. (2024). Adenosine-Dependent Arousal Induced by Astrocytes in a Brainstem Circuit. Adv Sci, 11: e2407706.

[8] Fink K, Zorec R, Kreft M (2025). Cannabinoid Ligand-Mediated Glycogen Depletion in Astrocytes Is Associated with Increased Intracellular Calcium, Energy Metabolism, and Membrane Dynamics. J Neurochem, 169:e70332.

[9] Fink K, Velebit J, Vardjan N, Zorec R, Kreft M (2021). Noradrenaline-induced l-lactate production requires d-glucose entry and transit through the glycogen shunt in single-cultured rat astrocytes. J Neurosci Res, 99:1084–1098.

[10] Barros LF (2013). Metabolic signaling by lactate in the brain. Trends Neurosci, 36:396–404.

[11] Smith D, Pernet A, Hallett WA, Bingham E, Marsden PK, Amiel SA (2003). Lactate: a preferred fuel for human brain metabolism in vivo. J Cereb Blood Flow Metab, 23:658–664.

[12] DeBerardinis RJ, Lum JJ, Hatzivassiliou G, Thompson CB (2008). The biology of cancer: metabolic reprogramming fuels cell growth and proliferation. Cell Metab, 7:11–20.

[13] Verkhratsky A, Butt A (2007). Glial neurobiology: a textbook: John Wiley & Sons.

[14] Pellerin L, Magistretti PJ (1994). Glutamate uptake into astrocytes stimulates aerobic glycolysis: a mechanism coupling neuronal activity to glucose utilization. Proc Natl Acad Sci U S A, 91:10625–10629.

[15] Dembitskaya Y, Piette C, Perez S, Berry H, Magistretti PJ, Venance L (2022). Lactate supply overtakes glucose when neural computational and cognitive loads scale up. Proc Natl Acad Sci U S A, 119:e2212004119.

[16] Suzuki A, Stern SA, Bozdagi O, Huntley GW, Walker RH, Magistretti PJ, et al. (2011). Astrocyte-neuron lactate transport is required for long-term memory formation. Cell, 144:810–823.

[17] Bonvento G, Bolanos JP (2021). Astrocyte-neuron metabolic cooperation shapes brain activity. Cell Metab, 33:1546–1564.
[18] Brown AM (2004). Brain glycogen re-awakened. J Neurochem, 89:537–552.
[19] Clasadonte J, Scemes E, Wang Z, Boison D, Haydon PG (2017). Connexin 43-mediated astroglial metabolic networks contribute to the regulation of the sleep-wake cycle. Neuron, 95: 1365-1380.e5.
[20] Gibbs ME (2016). Role of glycogenolysis in memory and learning: regulation by noradrenaline, serotonin and ATP. Front Integr Neurosci, 9:70.
[21] Hertz L, Chen Y (2018). Glycogenolysis, an astrocyte-specific reaction, is essential for both astrocytic and neuronal activities involved in learning. Neuroscience, 370:27–36.
[22] Le Douce J, Maugard M, Veran J, Matos M, Jégo P, Vigneron P-A, et al. (2020). Impairment of glycolysis-derived l-serine production in astrocytes contributes to cognitive deficits in Alzheimer's disease. Cell Metab, 31:503-517.e8.
[23] Magistretti PJ, Allaman I (2018). Lactate in the brain: from metabolic end-product to signalling molecule. Nat Rev Neurosci, 19:235–249.
[24] Sun W, Liu Z, Jiang X, Chen MB, Dong H, Liu J, et al. (2024). Spatial transcriptomics reveal neuron–astrocyte synergy in long-term memory. Nature, 627:374–381.
[25] Cataldo AM, Broadwell RD (1986). Cytochemical identification of cerebral glycogen and glucose-6-phosphatase activity under normal and experimental conditions: I. Neurons and glia. J Electron Microsc Tech, 3:413–437.
[26] Wender R, Brown AM, Fern R, Swanson RA, Farrell K, Ransom BR (2000). Astrocytic glycogen influences axon function and survival during glucose deprivation in central white matter. J Neurosci, 20:6804–6810.
[27] Stickgold R (2005). Sleep-dependent memory consolidation. Nature, 437:1272–1278.
[28] Benington JH, Heller HC (1995). Restoration of brain energy metabolism as the function of sleep. Prog Neurobiol, 45:347–360.
[29] DiNuzzo M, Nedergaard M (2017). Brain energetics during the sleep–wake cycle. Curr Opin Neurobiol, 47:65–72.
[30] Guthrie PB, Knappenberger J, Segal M, Bennett MV, Charles AC, Kater SB (1999). ATP released from astrocytes mediates glial calcium waves. J Neurosci, 19:520–528.
[31] Pangrsic T, Potokar M, Stenovec M, Kreft M, Fabbretti E, Nistri A, et al. (2007). Exocytotic release of ATP from cultured astrocytes. J Biol Chem, 282:28749–28758.
[32] Halassa MM, Fellin T, Haydon PG (2009). Tripartite synapses: roles for astrocytic purines in the control of synaptic physiology and behavior. Neuropharmacology, 57:343–346.
[33] Iliff BW, Swoap SJ (2012). Central adenosine receptor signaling is necessary for daily torpor in mice. Am J Physiol Regul Integr Comp Physiol, 303:R477–R484.
[34] Pascual O, Casper KB, Kubera C, Zhang J, Revilla-Sanchez R, Sul J-Y, et al. (2005). Astrocytic purinergic signaling coordinates synaptic networks. Science, 310:113–116.
[35] Fields RD, Burnstock G (2006). Purinergic signalling in neuron–glia interactions. Nat Rev Neurosci, 7:423–436.
[36] Haydon PG (2017). Astrocytes and the modulation of sleep. Curr Opin Neurobiol, 44:28–33.
[37] Theparambil SM, Kopach O, Braga A, Nizari S, Hosford PS, Sagi-Kiss V, et al. (2024). Adenosine signalling to astrocytes coordinates brain metabolism and function. Nature, 632:139–146.
[38] Allaman I, Lengacher S, Magistretti PJ, Pellerin L (2003). A2B receptor activation promotes glycogen synthesis in astrocytes through modulation of gene expression. Am J Physiol Cell Physiol, 284:C696–C704.
[39] Petit J-M, Gyger J, Burlet-Godinot S, Fiumelli H, Martin J-L, Magistretti PJ (2013). Genes involved in the astrocyte-neuron lactate shuttle (ANLS) are specifically regulated in cortical astrocytes following sleep deprivation in mice. Sleep, 36:1445–1458.
[40] Madeira D, Dias L, Santos P, Cunha RA, Canas PM, Agostinho P (2021). Association between adenosine A2A receptors and connexin 43 regulates hemichannels activity and ATP release in astrocytes exposed to amyloid-β peptides. Mol Neurobiol, 58:6232–6248.
[41] Orr AG, Hsiao EC, Wang MM, Ho K, Kim DH, Wang X, et al. (2015). Astrocytic adenosine receptor A2A and Gs-coupled signaling regulate memory. Nat Neurosci, 18:423–434.
[42] Nishizaki T (2004). ATP- and adenosine-mediated signaling in the central nervous system: adenosine stimulates glutamate release from astrocytes via A2a adenosine receptors. J Pharmacol Sci, 94:100–102.
[43] Bellesi M, de Vivo L, Tononi G, Cirelli C (2015). Effects of sleep and wake on astrocytes: clues from molecular and ultrastructural studies. BMC Biol, 13:66.
[44] Chatton JY, Marquet P, Magistretti PJ (2000). A quantitative analysis of l-glutamate-regulated Na+ dynamics in mouse cortical astrocytes: implications for cellular bioenergetics. Eur J Neurosci, 12:3843–3853.
[45] Pellerin L, Magistretti PJ (1997). Glutamate uptake stimulates Na+, K+-ATPase activity in astrocytes via activation of a distinct subunit highly sensitive to ouabain. J Neurochem, 69:2132–2137.
[46] Netchiporouk L, Shram N, Salvert D, Cespuglio R (2001). Brain extracellular glucose assessed by voltammetry throughout the rat sleep–wake cycle. Eur J Neurosci, 13:1429–1434.
[47] Dash MB, Tononi G, Cirelli C (2012). Extracellular levels of lactate, but not oxygen, reflect sleep homeostasis in the rat cerebral cortex. Sleep, 35:909–919.
[48] Naylor E, Aillon DV, Barrett BS, Wilson GS, Johnson DA, Johnson DA, et al. (2012). Lactate as a biomarker for sleep. Sleep, 35:1209–1222.
[49] Wisor JP, Rempe MJ, Schmidt MA, Moore ME, Clegern WC (2013). Sleep slow-wave activity regulates cerebral glycolytic metabolism. Cerebral Cortex, 23:1978–1987.
[50] Iliff JJ, Wang M, Liao Y, Plogg BA, Peng W, Gundersen GA, et al. (2012). A paravascular pathway facilitates CSF flow through the brain parenchyma and the

clearance of interstitial solutes, including amyloid β. Sci Transl Med, 4:147ra111.
[51] Xie L, Kang H, Xu Q, Chen MJ, Liao Y, Thiyagarajan M, et al. (2013). Sleep drives metabolite clearance from the adult brain. Science, 342:373–377.
[52] Schwarts JP, Wilson DJ (1992). Preparation and characterization of type 1 astrocytes cultured from adult rat cortex, cerebellum, and striatum. Glia, 5:75–80.
[53] Vardjan N, Kreft M, Zorec R (2014). Dynamics of β-adrenergic/cAMP signaling and morphological changes in cultured astrocytes. Glia, 62:566–579.
[54] Borea PA. 2009. A3 adenosine receptors from cell biology to pharmacology and therapeutics: Springer Science & Business Media.
[55] Eckle T, Krahn T, Grenz A, Köhler D, Mittelbronn M, Ledent C, et al. (2007). Cardioprotection by ecto-5′-nucleotidase (CD73) and A2B adenosine receptors. Circulation, 115:1581–1590.
[56] Goulding J, May LT, Hill SJ (2018). Characterisation of endogenous A2A and A2B receptor-mediated cyclic AMP responses in HEK 293 cells using the GloSensor™ biosensor: Evidence for an allosteric mechanism of action for the A2B-selective antagonist PSB 603. Biochem Pharmacol, 147:55–66.
[57] Hinz S, Lacher SK, Seibt BF, Müller CE (2014). BAY60-6583 acts as a partial agonist at adenosine A2B receptors. J Pharmacol Exp Ther, 349:427–436.
[58] Kuno A, Critz SD, Cui L, Solodushko V, Yang X-M, Krahn T, et al. (2007). Protein kinase C protects preconditioned rabbit hearts by increasing sensitivity of adenosine A2b-dependent signaling during early reperfusion. J Mol Cell Cardiol, 43:262–271.
[59] Dringen R, Karger G, Winkler U, Hirrlinger J (2025). ATP Metabolism of Astrocytes: Consumption, Regeneration and Restoration. Neurochem Res, 50:357.
[60] Rosenberg PA, Dichter MA (1985). Glycogen accumulation in rat cerebral cortex in dissociated cell culture. J Neurosci Methods, 15:101–112.
[61] Matos M, Augusto E, Santos-Rodrigues AD, Schwarzschild MA, Chen JF, Cunha RA, et al. (2012). Adenosine A2A receptors modulate glutamate uptake in cultured astrocytes and gliosomes. Glia, 60:702–716.
[62] Pelassa S, Guidolin D, Venturini A, Averna M, Frumento G, Campanini L, et al. (2019). A2A-D2 heteromers on striatal astrocytes: Biochemical and biophysical evidence. Int J Mol Sci, 20:2457.
[63] San Martín A, Ceballo S, Ruminot I, Lerchundi R, Frommer WB, Barros LF (2013). A genetically encoded FRET lactate sensor and its use to detect the Warburg effect in single cancer cells. PloS One, 8:e57712.
[64] Nikolaev VO, Bunemann M, Hein L, Hannawacker A, Lohse MJ (2004). Novel single chain cAMP sensors for receptor-induced signal propagation*♦. J Biol Chem, 279:37215–37218.
[65] Dolanc D, Zorec TM, Smole Z, Maver A, Horvat A, Pillaiyar T, et al. (2022). The activation of GPR27 increases cytosolic L-lactate in 3T3 embryonic cells and astrocytes. Cells, 11:1009.
[66] Turovsky EA, Braga A, Yu Y, Esteras N, Korsak A, Theparambil SM, et al. (2020). Mechanosensory signaling in astrocytes. J Neurosci, 40:9364–9371.
[67] Alexander SP, Fabbro D, Kelly E, Mathie A, Peters JA, Veale EL, et al. (2019). The concise guide to pharmacology 2019/20: Enzymes. Br J Pharmacol, 176:S297–S396.
[68] Borea PA, Gessi S, Merighi S, Vincenzi F, Varani K (2018). Pharmacology of adenosine receptors: the state of the art. Physiol Rev, 98:1591–1625.
[69] Fredholm BB, IJzerman AP, Jacobson KA, Klotz K-N, Linden J (2001). International Union of Pharmacology. XXV. Nomenclature and classification of adenosine receptors. Pharmacol Rev, 53:527–552.
[70] Biber K, Klotz K-N, Berger M, Gebicke-Härter PJ, van Calker D (1997). Adenosine A1 receptor-mediated activation of phospholipase C in cultured astrocytes depends on the level of receptor expression. J Neurosci, 17:4956–4964.
[71] Boison D, Chen J-F, Fredholm BB (2010). Adenosine signaling and function in glial cells. Cell Death Differ, 17:1071–1082.
[72] Franco R, Rivas-Santisteban R, Reyes-Resina I, Navarro G (2021). The old and new visions of biased agonism through the prism of adenosine receptor signaling and receptor/receptor and receptor/protein interactions. Front Pharmacol, 11:628601.
[73] Kiyoshi CM, Zhou M (2019). Astrocyte syncytium: a functional reticular system in the brain. Neural Regen Res, 14:595–596.
[74] Sobolczyk M, Boczek T (2022). Astrocytic calcium and cAMP in neurodegenerative diseases. Front Cell Neurosci, 16:889939.
[75] Fink K, Prebil ML, Vardjan N, Jensen J, Zorec R, Kreft M (2020). Increase in Subcellular Gsk-3 Clusters in Insulin- and Adrenaline-Treated Differentiated Rat Skeletal Muscle Fibres. Image Anal Stereol, 39:25–32.